LITHOS 532–533 (2026) 108511

Contents lists available at ScienceDirect

LITHOS

journal homepage: www.elsevier.com/locate/lithos

Thermal and fluid evolution during contact metamorphism around the Kevitsa and Satovaara intrusions: implications for sulfur and metal mobilization in the host black schist

V.J. Virtanen [a,b,*], H.R. Campos Rodríguez [a], S. Yang [c], G. Iacono-Marziano [a], T. Voipio [d], A. Canizarès [e], Y. Gourseaud [a], M. Versavel [a], T. Törmälehto [d]

[a] Institut des Sciences de la Terre d'Orléans, UMR 7327, Université d'Orléans, CNRS, BRGM, OSUC, Orléans, France
[b] Department of Geosciences and Geography, University of Helsinki, Helsinki, Finland
[c] Oulu Mining School, University of Oulu, Oulu, Finland
[d] Boliden Kevitsa Mining Oy, Sodankylä, Finland
[e] Conditions Extrêmes et Matériaux - Haute Température et Irradiation, UPR 3079, Université d'Orléans, CNRS, Orléans, France

ARTICLE INFO

Keywords:
Contact metamorphism
Black schist
Sulfide deposit
Hydrothermal processes
Raman spectroscopy
Carbonaceous materials

ABSTRACT

Contact metamorphism of carbon- and sulfur-rich black schists can play a critical role in the genesis of magmatic sulfide deposits. This study investigates the metamorphic evolution of the Matarakoski formation black schist surrounding the Kevitsa and Satovaara intrusions in northern Finland. Raman spectroscopy of carbonaceous materials and Ti-in-biotite thermometry indicate peak contact metamorphic temperatures of 500–600 ± 50 °C. Biotite-scapolite alteration during contact metamorphism indicates influx of Cl-rich fluids, which mobilized Cu and Co within the black schist and possibly into the Kevitsa intrusion. These fluids were channelized in porous zones created by the sills adjacent to the Kevitsa intrusion. During contact metamorphism, pyrite decomposition to pyrrhotite released sulfur, potentially contributing to the Kevitsa Cu-Ni-PGE deposit. Minor hydrothermal sulfides, including Co-rich pyrite, chalcopyrite, and arsenopyrite, suggest fluid-mediated metal redistribution during retrograde metamorphism. These findings support a multi-stage model of ore formation involving partial melting, devolatilization, and hydrothermal fluid transport, emphasizing the significance of contact aureole processes in magmatic sulfide systems.

1. Introduction

Assimilation of carbonaceous material- and sulfide-rich unconsolidated sediments and (meta)sedimentary rocks, by mafic-ultramafic magmas is widely recognized as an important process in the genesis of magmatic sulfide deposits. Notably, assimilation of sulfide-rich black shales contributed to the formation of the Cu-Ni(-PGE) sulfide deposits of the Duluth Complex in Minnesota, USA (e.g., Ripley, 1981; Queffurus and Barnes, 2014; Virtanen et al., 2024), the Kabanga Ni-Cu(-PGE) deposits in Tanzania (Maier and Barnes, 2010), the Ni—Cu sulfide deposits of the Pechenga intrusion in Kola Peninsula (e.g., Barnes et al., 2001; Hanski et al., 2011), and the Cu-Ni-PGE deposit of Kevitsa in Lapland, Finland (Grinenko et al., 2003; Luolavirta et al., 2018a, 2018b, 2018c; Mutanen, 1997). Magmas can assimilate sulfur from black shales through devolatilization fluids and selective or bulk assimilation (e.g., Barnes et al., 2001; Mutanen, 1997; Queffurus and Barnes, 2014) depending on the sulfide mineralogy and composition of the host rock (Virtanen et al., 2021, 2024). Therefore, constraining the contact metamorphic processes in the host rocks is essential for understanding the mechanisms of sulfur mobilization, transfer, and assimilation in magmatic sulfide systems.

The Kevitsa intrusion (Fig. 1) is a 2.05 Ga ultramafic-mafic cumulate body hosting an ore-grade deposit of disseminated Cu-Ni-PGE sulfides (Grinenko et al., 2003; Luolavirta et al., 2018a, 2018b, 2018c; Mutanen, 1997) with indicated remaining resources of 111.3 Mt. at 0.23 wt% Ni, 0.34 wt% Cu, 0.010 wt% Co, 0.12 ppm Pt, 0.07 ppm Pd, and 0.07 ppm Au (Boliden, 2024, https://investors.boliden.com/sites/boliden-ir/files/pr/202503192744-1.pdf, site visited on September 05, 2025). Another ultramafic–mafic intrusion east of Kevitsa, known as Satovaara (Fig. 1), is likely genetically related to Kevitsa but contains only minor

* Corresponding author at: 1A Rue de la Ferollerie, F-45071 Orléans, France.
E-mail address: ville.virtanen@cnrs-orleans.fr (V.J. Virtanen).

https://doi.org/10.1016/j.lithos.2026.108511
Received 10 October 2025; Received in revised form 12 February 2026; Accepted 16 March 2026
Available online 21 March 2026

sulfide deposits (Mutanen, 1997). Both intrusions are hosted within the Savukoski Group, which mostly consists of the sulfide-rich black schists known as the Matarakoski formation as well as komatiitic to mafic volcanic rocks (Fig. 1; Köykkä et al., 2019). The host black schists are thought to have contributed external sulfur to the magma of the Kevitsa intrusion, promoting sulfide saturation and ore formation (Grinenko et al., 2003; Luolavirta et al., 2018a; Mutanen, 1997). Nonetheless, the mineralogy and contact metamorphism of the black schists are poorly constrained.

This study investigates the contact metamorphism of the Matarakoski formation black schist surrounding the Kevitsa and Satovaara intrusions in northern Finland. We constrain peak metamorphic temperatures and present detailed mineral chemistry and whole-rock geochemical data to evaluate the contact metamorphic processes. Our findings emphasize the role of Cl-bearing fluids in mobilizing metals during the contact metamorphism. We also provide a paragenetic model for the sulfides in the contact-metamorphosed black schist.

1.1. Geological setting

The Matarakoski formation belongs to the Savukoski Group, which consists of various sedimentary and volcanic rocks that were deposit between 2.15 and 2.05 Ga based on field relationships with cross-cutting intrusions (Räsänen and Huhma, 2001; Köykkä et al., 2019). Stratigraphically, the Savukoski Group is above the Sodankylä Group, which consists of conglomerates, arkosic quartzites, pelites, carbonate and sulfate evaporites as well as mafic volcanic rocks, which were deposited between ~2.38 Ga and 2.15 Ga in a *syn-* to post-rift setting (Haverinen, 2020; Köykkä et al., 2019). The presence of halite pseudomorphs indicate that salt beds could have existed in the original stratigraphy (Haverinen, 2020). The Savukoski Group represents a sedimentary basin in a passive margin setting (Köykkä et al., 2019). Carbon and sulfur-rich black schists and greywackes of the Matarakoski formation are present at the base of the Savukoski Group and the upper part mainly consists of komatiitic to picritic lavas and mafic tuffs (Haverinen, 2020; Köykkä et al., 2019). Traditionally, the carbon and sulfur-bearing pelitic rocks of Matarakoski formation have been divided into black schists and phyllites on the basis that the former contains generally more sulfides and causes staining on skin contact due to the abundant carbonaceous materials (Lehtonen et al., 1998). Here, we refer to these rocks collectively as black schists as they both contain generally >0.5 wt% C, which has been suggested as the lower limit for the use of the prefix black for shales and schists (Huyck, 1991).

The Savukoski Group was deformed and metamorphosed during the Lapland-Kola (Daly et al., 2006), Lapland-Norrbotten, and Svecofennian (Lahtinen et al., 2005) orogenies, which caused greenschist to lower amphibolite facies regional metamorphism of the rocks (Hölttä and Heilimo, 2017; Sayab et al., 2021). The black schists of the Matarakoski formation often preserve structural and compositional features of the original sedimentary layering (Hölttä et al., 2007; Mikkola, 1941). The typical mineral assemblages include (i) chlorite, white mica, quartz, ilmenite, and pyrite ± plagioclase ± biotite ± rutile ± tourmaline ± monazite as well as (ii) biotite, chlorite, quartz, ilmenite, and pyrite ± rutile ± titanite ± carbonate minerals ± scapolite (Hackman, 1927; Mikkola, 1941; Tyrväinen, 1983; Lehtonen et al., 1998; Hölttä et al., 2007). Biotite and chlorite are typically in the groundmass but locally present as up to 0.05–0.1 mm porphyroblasts (Tyrväinen, 1983; Lehtonen et al., 1998; Hölttä et al., 2007). Based on chlorite thermometry, the schists and metavolcanic rocks north of Sodankylä experienced regional metamorphic temperatures in the range of 350–400 °C (Hölttä et al., 2007). Pyrite with a suggested sedimentary origin is present as macroscopic concretions and as up to one-centimeter thick regular bands, which can constitute >10 wt% of the schist (Lehtonen et al., 1998; Mikkola, 1941). Scapolite porphyroblasts, which can reach size of roughly one centimeter, are present locally and they possibly formed due to infiltration of Cl-rich fluids from the regionally common evaporite rocks of the Sodankylä Group (Hackman, 1927; Haverinen, 2020; Lehtonen et al., 1998; Tuisku, 1985; Tyrväinen, 1983). Scapolite porphyroblasts in the black schists are particularly abundant near the Kevitsa intrusion (Lehtonen et al., 1998; Mutanen, 1997). The formation of scapolite porphyroblasts is not lithologically controlled and they are present in a wide range of rocks with both sedimentary and igneous origin. In fact, scapolitized rocks are present throughout the northern Fennoscandia, along a ~ 50–100 km wide east-west oriented zone

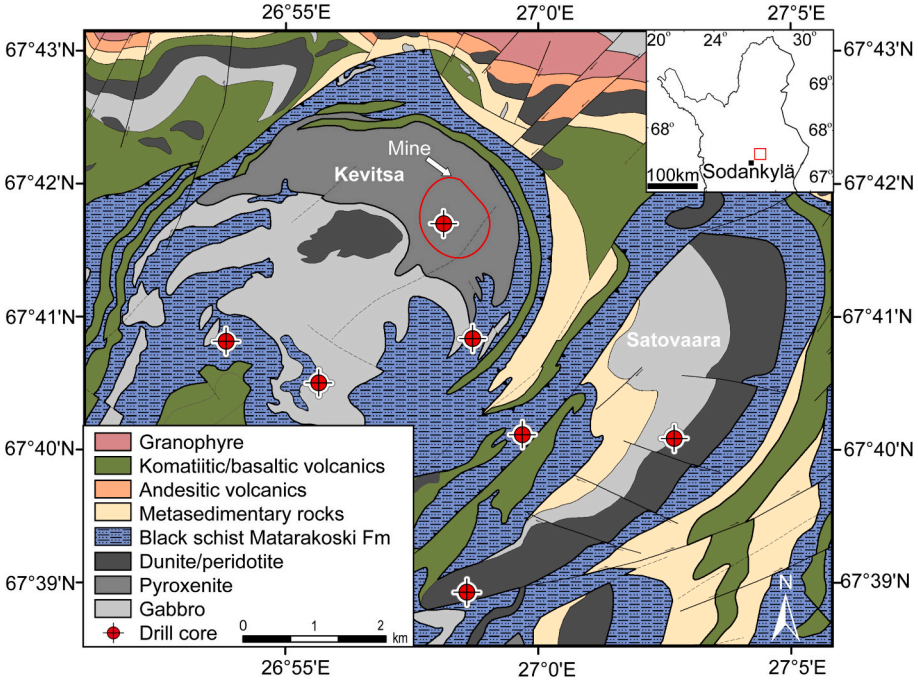

Fig. 1. A geological map of the study area indicating the locations of the drill cores sampled for the Matarakoski black schist. The drill core names are not shown due to data confidentiality.

extending from the eastern border of Finland to the western border of Sweden (Frietsch et al., 1997).

In the study area, the Kevitsa and Satovaara intrusions intersect the Matarakoski formation (Fig. 1; Mutanen, 1997, Luolavirta et al., 2018a, 2018b, 2018c). Satovaara is a concordant intrusion with ultramafic basal cumulates and upper gabbroic rocks (Fig. 1). Compared to the Kevitsa intrusion, Satovaara contains higher proportion of olivine-rich ultramafic rocks, the surrounding contact-aureole is thinner, and the Cu-Ni-PGE sulfide mineralization is restricted to sporadic cloud-like, possibly stratigraphically bound, zones consisting of disseminated sulfides (Mutanen, 1997). Kevitsa is a shallow conduit-type intrusion consisting of ultramafic, mostly pyroxenitic, and gabbroic cumulates (Mutanen, 1997, Luolavirta et al., 2018b, 2018c, Schoneveld et al., 2025). Incompatible trace elements concentrations even in the most evolved cumulates of Kevitsa (Luolavirta et al., 2018a, 2018b) are similar or lower compared to the proposed picritic parental melt (see Hanski and Kamenetsky, 2013), which indicates that much of the residual melt was expelled from the intrusion. The Kevitsa intrusion experienced an extended period of magmatic replenishment (Luolavirta et al., 2018a, 2018b, 2018c; Schoneveld et al., 2025), which possibly explains the thicker contact metamorphic aureole compared to the Satovaara intrusion. Little is known about the extent of assimilation in Satovaara but Kevitsa intrusion is thoroughly contaminated based on radiogenic Sr ($^{87}Sr/^{86}Sr_i = 0.7050–0.7109$: Luolavirta et al., 2018a) and Nd isotopic ($\varepsilon Nd_i = -2.0$ to -6.9: Huhma et al., 2018) compositions in all rock types. Sporadically, the Kevitsa rocks contain unusual minor minerals including graphite and Cl-rich magmatic phases including amphibole, biotite, and apatite (Grinenko et al., 2003; Mutanen, 1997). The disseminated Cu-Ni(-PGE) sulfide deposits are hosted by the pyroxene-rich ultramafic cumulates. Based on the $\delta^{34}S$ composition of the sulfides within the deposit, assimilation of sulfur from a sedimentary source was important for the formation of the deposit (Grinenko et al., 2003; Luolavirta et al., 2018a). Sulfur and carbon isotopes from the Kevitsa intrusion are compatible with the Matarakoski formation being the main sedimentary sulfur source (Grinenko et al., 2003).

In the vicinity of the Kevitsa intrusion, the black schist of the Matarakoski formation has been divided into two units based on the abundances of sulfides and carbonaceous materials (Grinenko et al., 2003). In the stratigraphically lower unit of the black schist, sulfide and carbonaceous material contents increase upwards. The stratigraphically upper unit has relatively higher sulfide but lower carbonaceous material contents relative the lower unit. As opposed to the regional Matarakoski formation, where pyrite is the dominant sulfide (Hackman, 1927; Mikkola, 1941), the main sulfide mineral in the black schist near Kevitsa intrusion is pyrrhotite, while pyrite and chalcopyrite are the most common minor minerals. The Kevitsa intrusion is hosted in the upper unit of the Matarakoski black schist with locally concordant (Lehtonen et al., 1998) and locally discordant contacts (Grinenko et al., 2003; Mutanen, 1997).

In addition to hosting the mineralized Kevitsa and Satovaara intrusions, the black schists of the Matarakoski formation together with the overlying komatiitic rocks are among the main stratigraphic loci for polymetallic Au-deposits in Central Lapland (Eilu, 2015; Korkalo, 2006). These deposits are heterogeneous in terms of metal association ranging from the typical Au ± Ag ± Cu deposits to more anomalous Au ± Ag ± Cu ± Ni ± Co ± Sb deposits (Eilu, 2015; Korkalo, 2006). Especially, the anomalous Ni—Co assemblages are spatially associated with the komatiites overlying the Matarakoski formation black schist (Eilu, 2015). These polymetallic deposits may have formed in volcanogenic massive sulfide (VMS) or orogenic Au-type mineralization processes or as a combination of the two (Eilu, 2015). Metal enrichment seems to be often related to albitization ± scapolitization and to mm to m-scale veins composed of Fe-rich dolomite and quartz (Eilu, 2015; Frietsch et al., 1997; Korkalo, 2006). It should be noted that on the regional scale, from Finland to Sweden, several types of alteration-mineralization associations have been documented and that our description here is not meant to be exhaustive (for detailed studies see e.g., Frietsch et al., 1997;Eilu, 2015; Korkalo, 2006). It has been proposed that the carbonaceous materials caused reduction-induced precipitation of metals from an infiltrating saline fluid based on the leaching of carbon from the albitized and scapolitized black schists at the vicinity of the polymetallic deposits (Frietsch et al., 1997). The main ore minerals in these deposits are pyrrhotite, pyrite, and chalcopyrite with minor arsenopyrite, gersdorffite, cobaltite, and pentlandite (Eilu, 2015; Korkalo, 2006). In addition, magnetite, native gold, Au—Ag tellurides, bismuthinides, molybdenite, millerite, violarite, and stibnite are present locally (Korkalo, 2006; Eilu, 2015).

2. Materials and methods

2.1. Sampling

We reviewed eight drill cores with a total of >900 m of black schist near the Kevitsa and Satovaara intrusions (Fig. 1). These drill cores contain black schists, of which some show non-fissile bedding with variably dark material (Fig. 2A), whereas others are characterized by primary sedimentary structures including mm-scale fissile bedding with alternating dark and light-colored material (Fig. 2B). Up to meter-scale intervals of nearly pure carbonaceous material are present sporadically (Fig. 2C). With the exception of the most carbon-rich horizons, all black schist types contain abundant macroscopically visible sulfides. Veins composed of quartz, carbonates, and sulfides commonly cross-cut the black schists (Fig. 2D). Collapse breccias within the black schists (Fig. 2E) possibly suggest dissolution of soluble interbeds such as salts, sulfates, or carbonates, or volume decrease due to dewatering of hydrate minerals such as gypsum. Near the Kevitsa intrusion, the black schists show gradual disappearance of the original bedding and increasing grain size, although the grains are still mostly <1 mm in diameter (Fig. 2F). In addition, the contact-metamorphic rocks show locally intensive scapolite-biotite alteration and loss of carbonaceous materials (Fig. 2F). At the contact zones, black schists and fine-grained intrusive rocks are often difficult to distinguish macroscopically.

In order to characterize the mineralogy and chemical composition of the Matarakoski formation, we collected 23 samples from the black schists from drill cores KV01–07 (Fig. 3): 15 from the massive portions (Fig. 2A), five from the thinly laminar portions (Fig. 2B), and three (K02, K07, and K11) from the horizons composed dominantly of carbonaceous materials (Fig. 2C). In the sampling, we avoided the cross-cutting quartz-carbonate-sulfide veins (Fig. 2D). The samples come from 0 to 165.5 m apparent distances (observed distance in the drill core) from intrusive rocks (Fig. 3). One sample (K02) is a xenolith, which comes from within the pyroxenitic part of the Kevitsa intrusion (not shown in Fig. 3). The most comprehensive sample set is from the drill core KV01 (Fig. 3) and contains variably scapolitized dark massive black schists (Fig. 2F) in contact with an albitized black schist and leucogabbro (Fig. 2G). The ten black schist samples from this drill core are from the contact and up to 62 m from it. From this drill core, we also collected four samples from the intrusive rocks: two fine-grained gabbroic rocks from 0 to 20 cm from the contact, a leucocratic medium-grained gabbroic rock 40 cm from the contact, and a melanocratic medium-grained gabbroic rock 2.2 m from the contact (Fig. 3). We produced polished thin sections from all samples. In addition, we acquired one sample of the regional black schist from Sattasrimpi, ~25 km south-west from Kevitsa, from the drill core archives of the Geological Survey of Finland to compare the types of carbonaceous materials on regional scale. This sample represents a quartz-poor chlorite mica schist layer with carbonaceous material-rich bands below a small peridotitic intrusive.

2.2. Raman spectroscopy

We used Raman spectroscopy to characterize the molecular structure

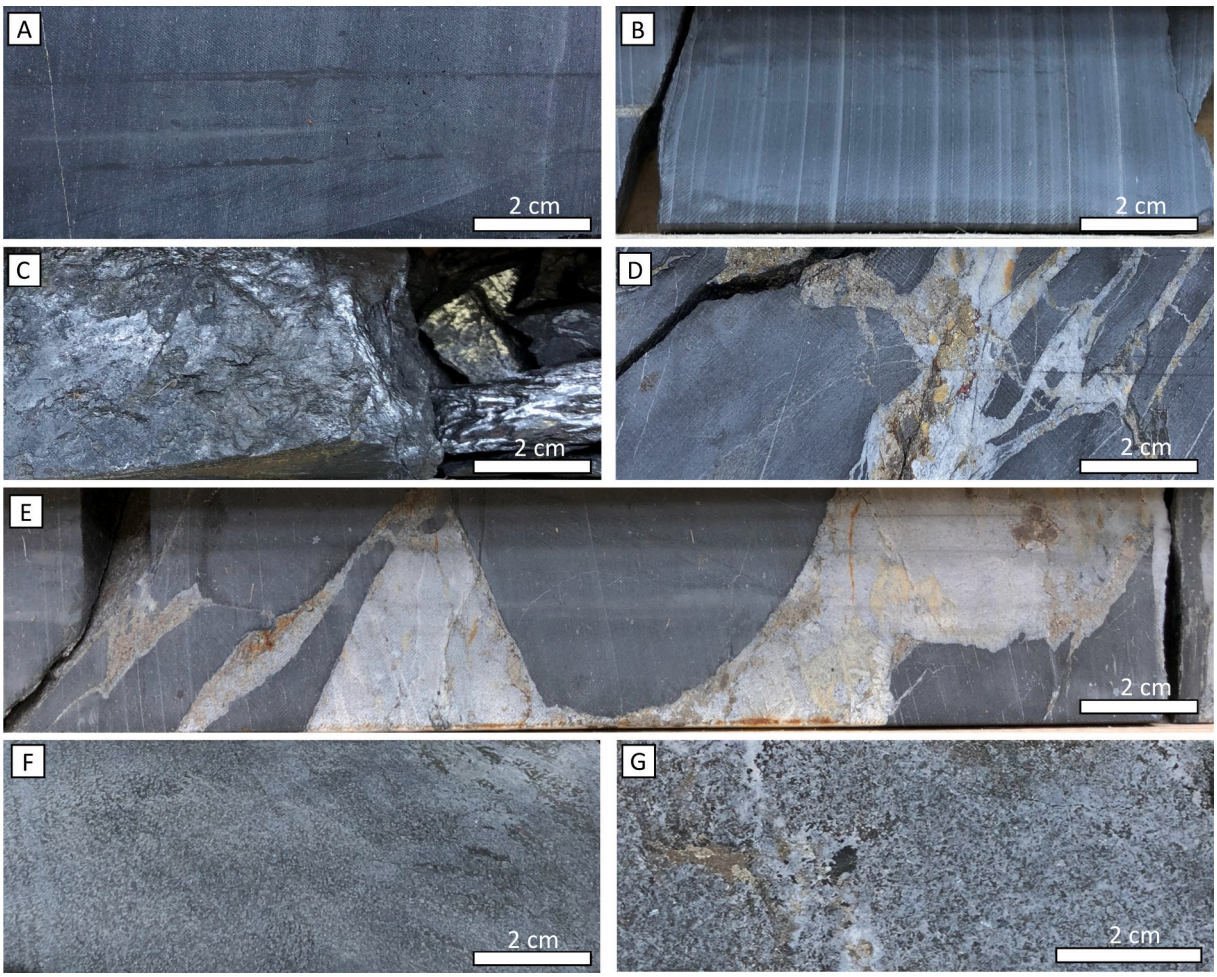

Fig. 2. Typical features in the Matarakoski formation: A) massive black schist, B) thinly laminated black schist, C) a horizon within thinly laminated black schist composed nearly purely of carbonaceous materials, D) quartz-carbonate-sulfide veins cross-cutting a black schist, E) a collapse breccia horizon within a black schist, F) thorougly biotite-scapolite-altered black schist with very low content of carbonaceous materials, and G) an albitized leucogabbro ~30 cm from the contact.

of the carbonaceous materials in the black schist samples. The Raman spectral features (i.e., energy distribution of scattered photons) of carbonaceous materials reflect bonding between connected C atoms and possibly other elements such as H, O, and S (for a comprehensive review, see Beyssac and Lazzeri, 2012). The main spectral features relevant for our study are (i) the so-called G band at 1580 cm^{-1}, which are related to graphite-like highly ordered stacked sheet structure, and (ii) the D1 and D2 bands at ~1340–1360 cm^{-1} and ~ 1620 cm^{-1}, respectively, which are related to structural defects and possibly the presence of elements other than C. On the basal plane of graphite sensu stricto, only the G band is present, whereas small D1 and D2 bands arise when measurements are done on the edge planes (Beyssac and Lazzeri, 2012). Several studies have shown that the molecular structure of the carbonaceous materials goes through systematic irreversible changes with increasing temperature, which makes the Raman spectroscopy of carbonaceous materials a useful method for determining metamorphic peak temperatures without the influence of retrograde resetting (e.g., Aoya et al., 2010; Beyssac et al., 2002; Lahfid et al., 2010).

We measured the carbonaceous materials using a Renishaw InVia Qontor confocal Raman microscope equipped with a 514.5 nm diode-pumped solid-state laser at the CEMHTI, Orléans. To focus the laser on the sample, we used a Leica DM2500 optical microscope with a 100× objective, which has a 0.85 numerical aperture providing a spatial resolution of ~0.75 μm. To avoid thermal damage of the carbonaceous materials, we set the laser power on sample surface to ~0.25 mW using a Thorlabs PM100A power meter. We applied an edge filter to filter out Rayleigh scattering and selected a grating with 1800 lines/mm to direct the signal to a thermo-electrically cooled (−70 °C) Renishaw Centrus PN200 CCD detector with a 1024 × 256 pixels array (26 × 26 μm pixel size). We used a silicon standard for detector calibration and a graphite standard to verify the absence of any spectral features related to heating.

We measured only carbonaceous materials that were present under transparent silicate and carbonate grains to avoid structural degradation caused by polishing. We recorded the spectrum for 30 s with five spectral accumulations (i.e., the total measurement time is 150 s for each spectrum) to reduce the noise. Because carbonaceous materials within samples can be heterogeneous (e.g. Aoya et al., 2010), we collected 15–16 spectra from each sample. For treatment of the raw measurement data, we used PeakFit (version 4.12). Linear or second order polynomial baselines were visually fitted to the measured spectra to define the signal background. Spectra affected by strong fluorescence causing a strongly curved background were discarded due to uncertainties in the fitting of the baseline. For spectral deconvolution, we fitted one or three symmetric peaks (i.e., G band ± D1 and D2 bands) to the measured spectra using the Voigt function. The fit between the fitted and measured spectra was generally $R^2 \geq 0.98$, which we adopted as the threshold value for including the data in the thermometry calculations. For thermometry, we adopted the parameterization of Beyssac et al. (2002) in which the peak temperature is calculated based on the surface area of the D1 peak relative to the total surface area of the spectrum: D1/(G + D1 + D2). This ratio is called the R2 parameter, which has been shown to linearly correlate with temperature following the relation T(°C) = −445 x R2 +

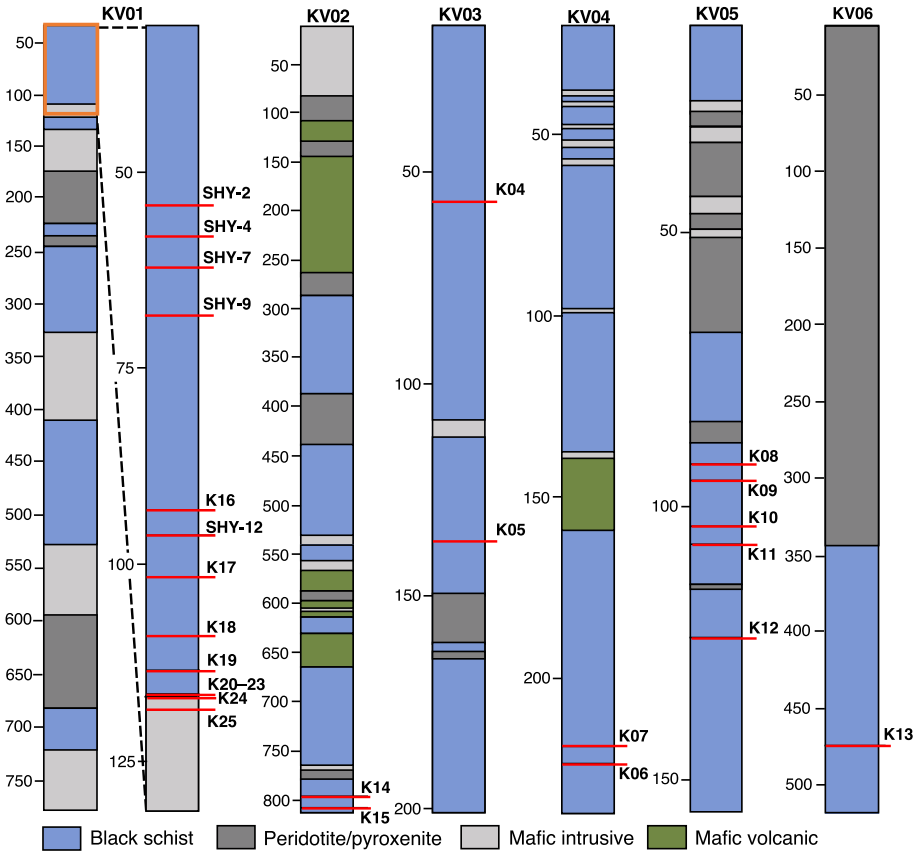

Fig. 3. Illustrations of the sampled drill cores, excluding the core KV07 from which only a xenolith (sample K02) within the main pyroxenite of the Kevitsa intrusion was collected.

641, and is valid over the temperature range 330–650 °C with an estimated uncertainty of ±50 °C (Beyssac et al., 2002). This thermometer has been calibrated with measurements done with a laser with the same wavelength as used in this study and has been shown to be valid for regionally metamorphosed and contact-metamorphic rocks (Aoya et al., 2010; Beyssac et al., 2002). The maximum temperature of the thermometer (650 °C) is defined by the temperature at which the carbonaceous materials reach perfectly ordered crystal structure of graphite.

2.3. Whole-rock geochemistry

With the exception of the samples from the horizons composed almost purely of carbonaceous materials, all black schist and igneous samples were included for the whole-rock geochemical analyses. From the xenolith samples, which also contained intrusive rocks, we only selected the black schist portion for the analyses. Sample preparation and analytical work was conducted by ALS Minerals. For major and trace element analyses, powdered samples were fused with lithium borate and subsequently digested in an acid solution. For base metal analyses, the lithium borate beads were digested using a four acid (HNO_3-HF-$HClO_4$-HCl) solution. The major elements were measured using inductively coupled plasma atomic emission spectrometry (ICP-AES), and trace elements using ICP mass spectrometry (MS). Loss on ignition was determined by weight loss after heating the sample powder to 1000 °C. Total C and S were measured from the powdered samples with infrared spectrometry using a LECO furnace. The amount of non-carbonate C was measured with the same method but the sample powders were leached multiple times using HCl before the measurement to remove carbonates from the analyte. Structurally bound water (H_2O^+) contents were measured from the sample powders with infrared spectrometry using a combustion furnace. To determine the analytical accuracy, precision, and detection limits, several standard materials and blanks were measured along the samples. More details of the whole-rock geochemistry methods are included in the ESM1.

2.4. Mineral chemical analyses

We conducted the mineral chemical analyses at the Institut des Sciences de la Terre d'Orléans. We used a Zeiss Merlin Compact field emission secondary electron microscope for imaging and qualitative phase identification. For quantitative measurements, we used a Cameca SX Five electron microprobe analyzer (EMPA) equipped with five wavelength-dispersive detectors. Chlorite, biotite, and scapolite compositions were measured from four black schist samples from the drill core KV01, which contains black schists at the contact with gabbroic rocks (Fig. 3). Twelve black schist samples from drill cores KV01–07 were included in sulfide composition measurements. For the measurements, we set the working distance to <10 mm and used a focused beam. For the silicate minerals, we used an acceleration voltage of 15 kV and current of 10 nA. For sulfides acceleration voltage was set to 20 kV and current to 40 nA. Detailed information about the analytical conditions, error calculation, and detection limits are included in the ESM1.

3. Results

3.1. Raman spectroscopy

In the thinly laminated and massive black schists, carbonaceous materials are present as equally dispersed rounded micron-scale disseminated grains within the groundmass and as elongated accumulations in fractures (Fig. 4A). These grains are structurally fairly homogeneous from sample to sample with the Raman spectra showing

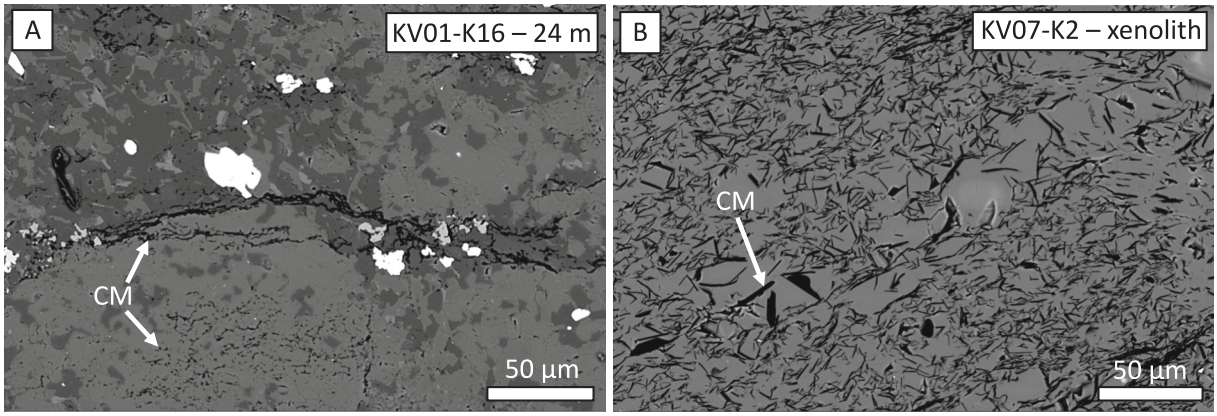

Fig. 4. Back-scattered electron (BSE) images showing occurrences of structurally disorganized (A) and fully graphitic (B) carbonaceous materials (black material indicated with CM) in the black schists of the Matarakoski formation.

well-developed G-bands with minor D1 and D2 bands (Fig. 5, Table S1). Raman spectroscopy reveals similar structural features for carbonaceous material in samples K07 and K11, which represent horizons composed almost entirely of carbon (Fig. 5). For the samples with this type of carbonaceous materials, we were able to measure 11–16 spectra, which complied with our criteria for baseline fitting and deconvolution (see methods). For most of these data, the average contribution of the D1 band on the sum spectra (R2 parameter) is 0.16–0.29 (Fig. 5) with a standard deviation of ≤0.06. The calculated average peak metamorphic temperatures for the samples are 513–566 °C (Fig. 5, Table S1) with the methodological uncertainty of ±50 °C. The R2 parameters in these samples near the Kevitsa intrusion are distinctly lower compared to the sample R58–35 from Sattasrimpi, which shows an average R2 of 0.42 indicating peak temperature of 456 ± 50 °C (Fig. 5, Table S1).

The intensively biotite-scapolite altered sample K18, which comes from 7.3 m distance from intrusive contact in drill core KV01 has very low concentration of C, hence we were able to measure only six spectra. For these spectra, average R2 is 0.19, which is slightly lower compared to most of the samples, although the data are partially overlapping (Fig. 5, Table S1). The calculated peak metamorphic temperature of this intensively biotite-scapolite altered sample is 556 ± 50 °C. From the same drill core the samples closer to the contact with the intrusive rocks (K19–20) contain too low concentrations of carbonaceous material for Raman measurements. The samples K14–15 from drill core KV02 contain micron-scale carbonaceous materials, which have more angular appearance compared to other samples. These materials yield distinctive

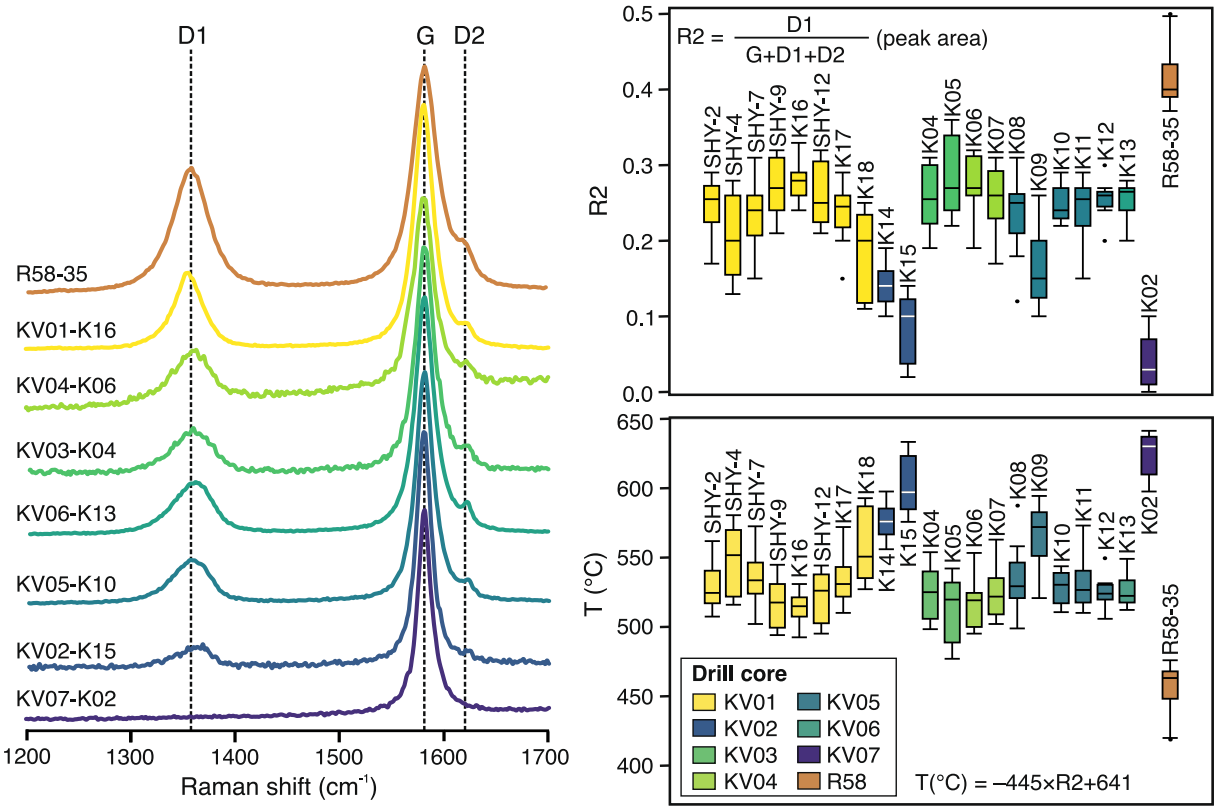

Fig. 5. Representative Raman spectra of carbonaceous materials from black schist of the Matarakoski Formation for each sampled drill core. Stippled lines indicate the ideal positions of the G, D1, and D2 peaks. Box plots summarize all measurements and present the calculated R2 parameter and corresponding peak metamorphic temperatures. All samples are from locations near the Kevitsa intrusion, except for sample R58–35, which was collected approximately 25 km southwest of Kevitsa.

Raman spectra with R2 of 0.10–0.16 and peak temperatures of 566–602 ± 50 °C (Fig. 5, Table S1). In addition, the xenolith sample K02 from within the pyroxenitic unit of the Kevitsa intrusion contains up to about 30 μm long lathlike grains of carbonaceous materials, which are present as one of the volumetrically major phases (Fig. 4B). Raman spectroscopic measurements of some grains show only a G band verifying that these lathlike grains are graphite sensu stricto (Fig. 5). Most measurements show small contributions from D1 and D2 bands (R2 is generally <0.05) due to the effect of orientation of the laths (Fig. 5, Table S1). The adopted thermometry indicates a minimum temperature of 641 °C (± 50 °C) for full graphitization (Beyssac et al., 2002) and the lower calculated temperatures (Fig. 5) arise from the orientation effect on the spectra. Hence, the presence of graphite in this xenolith indicates that the peak temperature exceeded ~650 °C.

3.2. Petrography and mineral chemistry of the black schist

The main silicate minerals in all black schist samples are chlorite, quartz, and biotite, which are present in variable grain sizes and proportions on the thin section scale, translating into the macroscopic bedding observable on the drill core scale. The abundance of carbonaceous materials is variable and governs the degree of dark coloration in the samples (Fig. 6A–B). Scapolite is a main mineral in some locations (Fig. 6C–D) and, in drill core KV01, it is the most abundant mineral in a 4 m thick interval next to thoroughly albitized black schist (Fig. 6D) and gabbro. Carbonaceous material is very scarce in the most intensively scapolitized rocks and completely absent in the albitized parts (Fig. 6C–D). The ubiquitous minor minerals are apatite and titanite, which are present in all samples, whereas plagioclase, and K-feldspar are locally present as minor and, less commonly, major minerals. Minor epidote and rutile are present in some samples. Chlorite, biotite, and typically elongated quartz grains are aligned with the foliation (Fig. 6E), which is close to parallel with the bedding. Locally, chlorite can also be found as round poikiloblasts, which preferentially enclose quartz grains. The schistosity bends around these poikiloblasts, which can reach up to 200–300 μm in diameter as opposed to ≤50 μm grains of chlorite in the groundmass.

In drill core KV01, chlorite and biotite in the groundmass are closer to their Mg end-member compositions with molar Mg/(Mg + Fe) of 0.58–0.80 (n = 12, Table S2) and 0.48–0.80 (n = 17, Table S3), respectively. The lowest Mg/(Mg + Fe) of biotite (0.48–0.69, n = 9 of 17) are measured near the intrusive contacts, where the original layering of the rock disappears. In the same drill core, scapolite forms rounded poikiloblasts (Fig. 6F), which can reach up to 500 μm in size. The structural formula of scapolite-group mineral can be written as (Ca, Na, K)$_4$(Si, Al)$_{12}$O$_{24}$(CO$_2$, SO$_2$, Cl) and the common end-members are Ca and C or S-rich meionite as well as Na and Cl-rich marialite. Meionite content of scapolite is calculated on molar basis as follows: Me = 100 * Ca/(Ca + Na + K). In our samples, meionite content varies from 25 to 35 and it is inversely linearly correlated with chlorine content (R^2 = 0.94), which varies between 2.6 and 3.7 wt% (molar content of 0.6–0.9 on stoichiometric basis) (Table S4). This means that the scapolite is marialitic. Qualitatively estimating, there is positive correlation between pervasiveness of scapolite alteration and Cl content of scapolite.

Among the common minor phases, apatite forms typically anhedral poikiloblasts, which can reach 300 μm in diameter. Compositionally it is fluorapatite based on qualitative EDS measurements. The other ubiquitous minor phase, titanite, is typically present as anhedral disseminated grains but also rarely as similar poikiloblasts as apatite. Of the less common minor phases, plagioclase (with the exclusion of albite) is present as ≤20 μm grains in the groundmass and it contains roughly equal amounts of CaO and Na$_2$O on the wt% basis based on EDS measurements. Potassium feldspar is present as similarly sized grains in the groundmass as plagioclase and shows spatial association with biotite.

3.3. Sulfide petrography and chemistry

Pyrrhotite is the most common sulfide mineral in our black schist

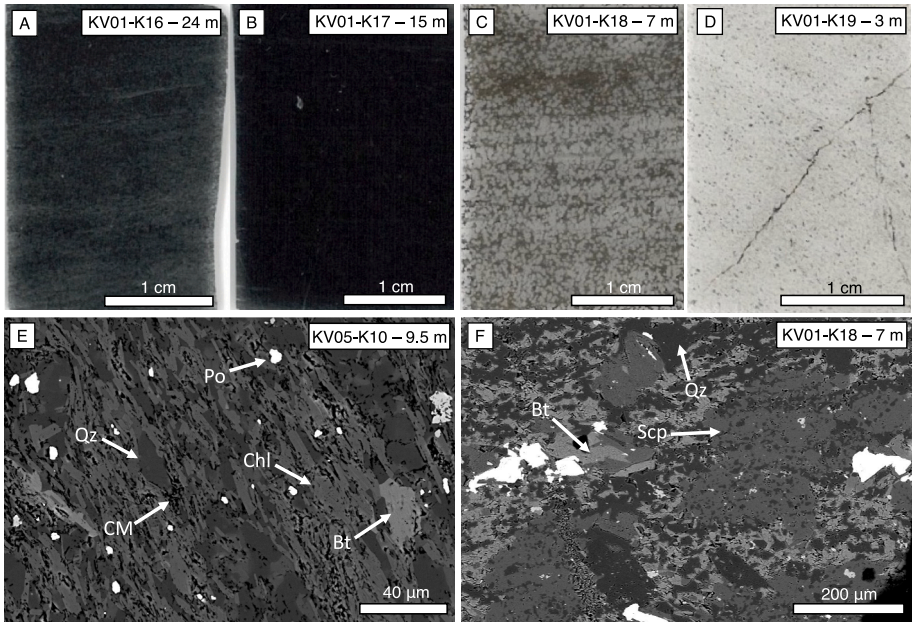

Fig. 6. Transmitted light scans of thin sections with black schist samples from drill core KV01: A) K16, 24 m from the intrusive contact with typical amount of carbonaceous materials (most of the opaque areas) and minor biotite-scapolite -overprint (light-colored bands), B) K17, 15 m from the intrusive contact showing high amount of carbonaceous materials, C) K18, 7 m from the intrusive contact showing pervasive biotite-scapolite alteration and nearly complete loss of carbonaceous materials (most of the dark parts are biotite), and D) K19, 3 m from the intrusive contact, with pervasive albitization, minor biotite-scapolite alteration, and complete loss of carbonaceous materials. The back-scattered electron images show samples E) K10, 9.5 m from the intrusive contact in drill core KV05 with the typical quartz-chlorite-biotite-pyrrhotite assemblage and carbonaceous materials (black) and F) K18 (same sample as in C) with scapolite porphyroblasts surrounded by biotite and quartz. The orientation of the original bedding is preserved in the quartz grains enclosed in scapolite. Note that the distances from intrusive contacts have been measured from a drill core, hence they are apparent and might not indicate a true distance.

samples and locally abundant enough to be considered as one of the main rock-forming minerals (> 5 vol%) (Fig. 7A–D). It is most commonly present as disseminated grains, which reach 400 μm in the longest dimension, but also as submicron inclusions within the poikiloblastic minerals. The disseminated grains are mostly elongated parallel with the schistosity (Fig. 7A) and they often contain small inclusions of the other groundmass minerals. The largest disseminated grains are commonly intergrown with the silicate minerals, mostly lath-like chlorite (Fig. 7D). Spatial association between disseminated pyrrhotite and titanite ± rutile is observed in some samples. Locally, the disseminated pyrrhotite grains contain troilite exsolutions, which are of submicron-scale and too small for EMPA measurements. Pyrrhotite is also locally present as <1 mm thick bands or veins, which are conformable with bedding and schistosity (Fig. 7A) and contain inclusions from the groundmass minerals. All types of pyrrhotite are variably Ni-bearing with the concentrations varying from 0.08 to 0.54 wt% (n = 146, Table S5). Pyrrhotite has generally fairly homogeneous Ni content on sample scale with the overall variability being close to the analytical uncertainty even between the coexisting disseminated and vein-like pyrrhotite. However, larger variability is observed in the most intensively biotite-scapolite altered sample, where Ni content in pyrrhotite is 0.19–0.54 wt% (n = 12), and from the two xenolith samples, where Ni contents in pyrrhotite are 0.09–0.28 wt% (n = 14) and 0.13–0.46 wt% (n = 12). In addition, one sample at the exact contact with an intrusive rock contains compositionally distinctive disseminated and vein-like pyrrhotite with 0.15–0.24 wt% Ni (n = 3) and 0.29–0.31 wt% (n = 8), respectively. There is no correlation between Ni content of pyrrhotite and the thermometry results.

The most common minor sulfide in our samples is chalcopyrite (Fig. 7B). It is mainly present as anhedral grains either at the flanks or within cracks of pyrrhotite grains. Minor element contents in chalcopyrite are below the detection limit of our microprobe measurements (Table S6). Arsenopyrite is the second most common minor sulfide in our black schist samples (Fig. 7C). It is present as inclusion-free grains within the groundmass and at the flanks of pyrrhotite grains. Arsenopyrite has variable concentrations of Co: 1.10–7.18 wt% and Ni: 0.06–0.92 wt% (Table S7). Pyrite is typically nearly euhedral but locally anhedral and present mainly within or at the flanks of the largest disseminated pyrrhotite grains (Fig. 7D) and pyrrhotite bands. Rarely, pyrite is also present as disseminated grains. Pyrite grains associated with pyrrhotite contain 0.59–1.57 wt% of Co, whereas Co content of the less common disseminated grains is below the detection limit (Table S8). Other less common minor sulfide phases include sphalerite, which has similar occurrence with chalcopyrite as well as galena and stibnite, which are sparsely present as small grains within the groundmass.

3.4. Whole-rock chemistry of the black schist and gabbro

Overall, the black schists of the Matarakoski formation are chemically heterogeneous (Table S9). Even with the exclusion of scapolitized (K18), albitized (K19–20), carbonate-rich (K09) and carbonaceous material-rich (K02) samples, most major elements show range of several weight percent: SiO_2 = 56.6–66.0 wt%, TiO_2, = 0.6–1.0 wt% Al_2O_3 = 11.0–17.5 wt%, $Fe_2O_3^{total}$ = 3.5–11.1 wt%, MgO = 2.9–7.0 wt%, CaO = 0.4–3.6 wt% Na_2O = 1.4–2.9 wt%, K_2O = 2.3–4.0 wt%, H_2O = 1.4–2.5 wt%, C_{org}, = 0.7–4.5 wt%, and S = 0.4–4.0 wt% (Table S9). In the drill core KV01, the black schist exhibits few clear changes in major elements towards the contact with the gabbroic intrusive rock (Fig. 8). The intensively scapolitized zone (3–7 m from the contact) shows depletion in C_{org} (0.07 wt%) and slightly elevated contents of CaO (3.5 wt%) and Na_2O (3.7 wt%) compared to black schists located farther from the intrusion in the same drill core and to most black schists in other cores (Fig. 8). More pronounced CaO (3.5–4.8 wt%) and Na_2O (7.6–7.7 wt%) enrichment as well as C_{org} (0.02 wt%) and K_2O (0.4–1.4 wt%) depletion is observed in the albitized zone (≤ 3 m from the contact) closer to the intrusive contact (Fig. 8). In addition, SiO_2 is slightly depleted in the black schist right next to the contact (Fig. 8). In terms of rare earth elements (REE) the samples from drill core KV01 have mostly similar light REE (LREE) enriched primitive mantle normalized (primitive mantle composition from Palme and O'Neill, 2013) patterns but absolute contents are lower compared to the black schists in other drill cores. The intensively scapolitized sample (K18) has lowest REE contents with a

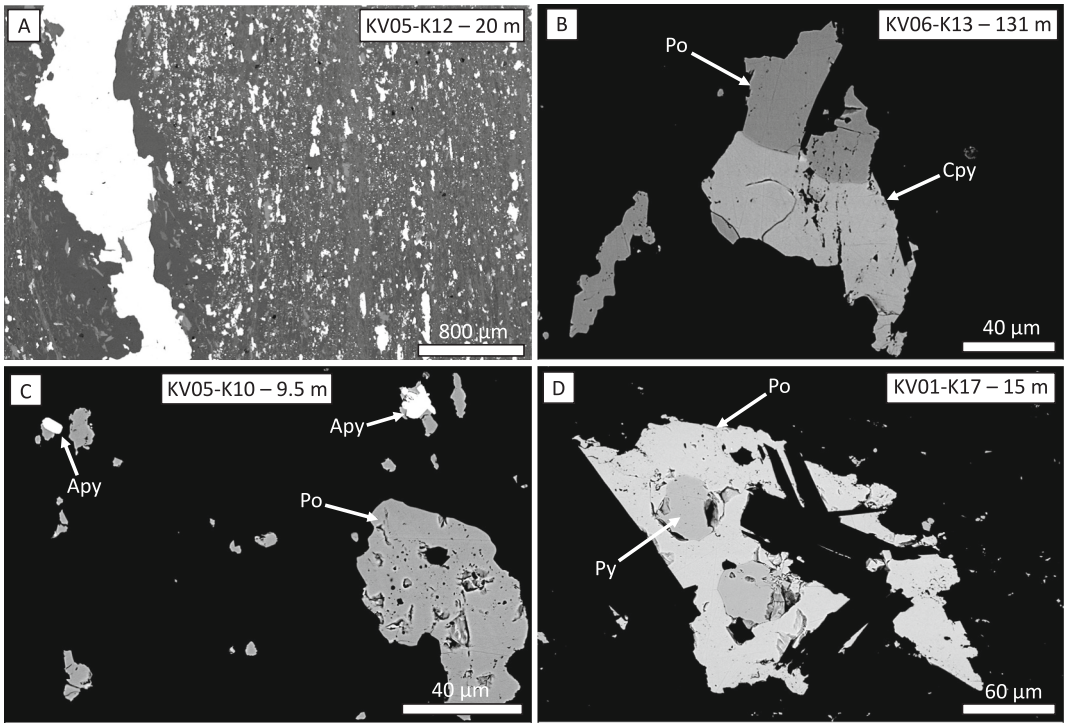

Fig. 7. Back-scattered electron images showing: A) typical occurrence of disseminated and lamina-type sulfides (white), B) pyrrhotite (Po) and chalcopyrite (Cpy), C) pyrrhotite and arsenopyrite (Apy), and) pyrrhotite and pyrite (Py). The titles indicate the sample and the apparent distance from an intrusive contact.

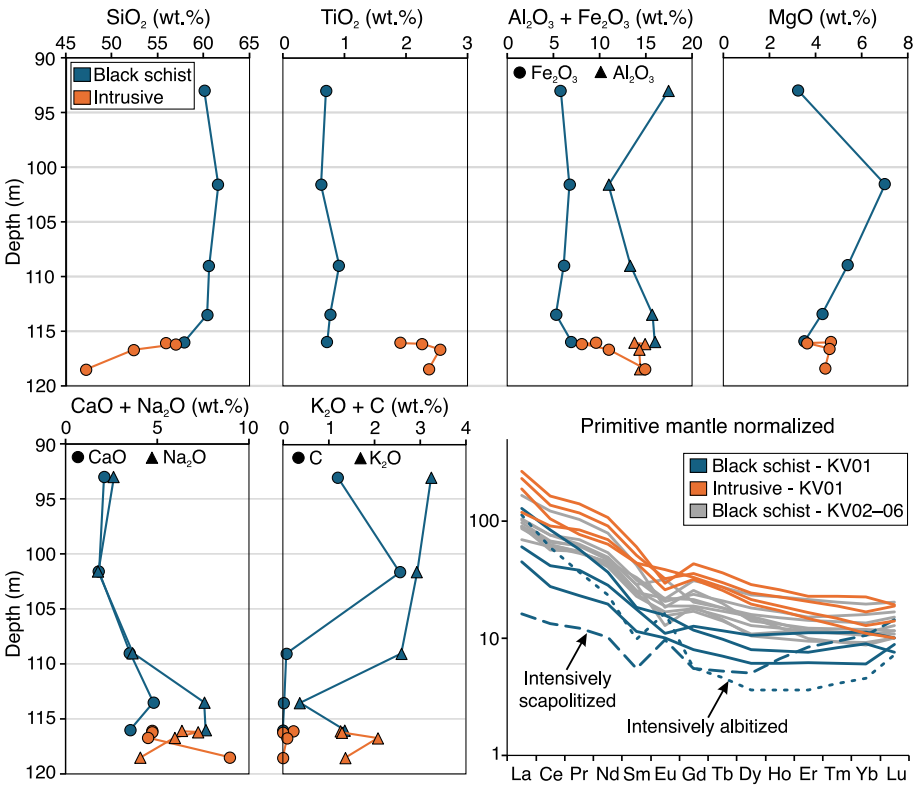

Fig. 8. Compositional variability in black schist and gabbroic intrusive rocks in drill core KV01. Rare earth element (REE) concentrations are normalized to primitive mantle values (Palme and O'Neill, 2013) and shown for all analyzed samples with the exception of the black schist xenolith K02.

distinct pattern showing low LREE, lower middle REE (MREE) but relatively high heavy REE (HREE), and a positive Eu anomaly (Fig. 8). The primitive mantle normalized pattern of the intensively albitized sample (K19) is characterized by highest LREE enrichment compared to MREE and HREE, slightly enriched Tm, Yb, and Lu compared to the other HREE, and a positive Eu anomaly (Fig. 8).

Compared to the black schist, the gabbroic rocks show clearer chemical differences towards the contact. Contents of SiO_2 and Na_2O are enriched, whereas TiO_2, Fe_2O_3, and CaO are depleted in the fine-grained gabbro and leucogabbro near the contact (Fig. 8). Notably, the gabbroic rocks have similar or lower MgO as well as higher TiO_2 and REE contents relative to most black schists in the area (Fig. 8). In addition, the gabbroic rocks have high Zr contents (160–294 ppm) compared to most of the black schists, which have 44–255 ppm Zr with an average of 115 ppm (Table S9).

4. Discussion

4.1. Peak metamorphism of black schist around the Kevitsa intrusion

It has been shown that heterogeneity of carbonaceous materials on thin section scale is one of the main sources of uncertainty in the Raman thermometry in both regionally metamorphosed and contact-metamorphosed rocks (Aoya et al., 2010; Lünsdorf et al., 2014). To account for this heterogeneity, it has been suggested that at least 25 and ideally >50 measurements should be conducted to calculate an average R2 parameter (see methods) for thermometry (Aoya et al., 2010), which is considerably more compared to our 11–16 spectra per sample. Aoya et al. (2010) showed that even >100 measurements from a single thin section may not be enough to reduce standard deviation of the R2 parameter to <0.06–0.07, which translates to an additional uncertainty of approximately ±30 °C on the thermometry. In our samples, the thin section scale standard deviation for the R2 parameter is 0.02–0.06 (Table S1), which we interpret to reflect relatively homogeneous populations of carbonaceous materials. It should be noted that Aoya et al. (2010) conducted measurements for 30–60 s with a single spectral accumulation, whereas we measured each spectrum for a total of 150 s (five accumulations of 30 s), which leads to better counting statistics for our spectra. In addition, Aoya et al. (2010) report laser power of 3 mW at the sample surface, which is considerably higher than the typically suggested ≤0.5 or 1 mW (≤ 0.25 mW in our study) to avoid heating-induced effects on photon scattering from carbonaceous materials (Beyssac and Lazzeri, 2012; Lünsdorf et al., 2014). We suggest that in the case of our samples and with the used analytical conditions, the 11–16 measured spectra are sufficient for calculating meaningful peak metamorphic temperatures.

Based on previous studies, the Savukoski Group, which hosts the Matarakoski formation, experienced greenschist facies regional metamorphic conditions with chlorite thermometry indicating temperatures of 350–400 °C ~ 10–15 km south of the Kevitsa intrusion (Hölttä et al., 2007, Hölttä and Heilimo, 2017). These estimates are similar to our measurements from the Matarakoski black schist sample originating ~25 km south-west from Kevitsa, which indicates a maximum peak metamorphic temperature of 460 ± 50 °C (Fig. 5). It should be noted, however, that our sample comes 17 m below an ultramafic intrusive rock with an undefined thickness (upper limit not observable), which may have caused some contact metamorphism. Only 1–2 km north of the Kevitsa intrusion, the degree of regional metamorphism reaches lower amphibolite facies, with an estimated peak pressure and temperature reaching 4–5 kbar and 560–615 °C, respectively (Hölttä et al., 2007; Hölttä and Heilimo, 2017). These conditions are found in rocks from the Sodankylä Group, which is stratigraphically below the Savukoski Group. Although our study area is located near the zone where regional metamorphism reached lower amphibolite facies conditions, we suggest that the peak metamorphic temperatures of 500–600 ± 50 °C (Fig. 5) recorded by our Matarakoski black schist samples from around the Kevitsa and Satovaara intrusions are more likely due to contact metamorphism. In the greenschist facies zone (south and southwest from the

Kevitsa intrusion), the pelitic rocks are characterized by chlorite–white mica–quartz ± plagioclase ± biotite and biotite–chlorite–quartz mineral assemblages (Hölttä et al., 2007). In the lower amphibolite facies zone (north of the Kevitsa intrusion), the typical mineral assemblages in the pelitic rocks are muscovite–chlorite–quartz and garnet–staurolite–muscovite–chlorite–quartz ± andalusite ± kyanite ± plagioclase, where the aluminosilicates are typically present as macroscopic porphyroblasts (Hölttä et al., 2007). Biotite is rare and mostly retrograde in the pelites metamorphosed at the lower amphibolite facies conditions (Hölttä et al., 2007). Our samples dominantly show a biotite–chlorite–quartz mineral assemblage, which is typical for the greenschist facies regional metamorphism.

To interpret the metamorphic history of our samples, we calculated a P-T pseudosection for an average composition of our Matarakoski black schist samples (Fig. 9A), using MAGEMin (Riel et al., 2022). The peak temperature constraints from the carbonaceous material thermometry and the complete absence of muscovite in our samples indicates that the stable peak metamorphic assemblage was alkali feldspar, plagioclase, biotite, cordierite, quartz, and rutile (Fig. 9A). This is compatible with the observed mineral assemblages from our samples with the exception of the lack of cordierite and presence of abundant chlorite and titanite (Fig. 6E and Fig. 9B–C). We suggest that the lack of cordierite is due to its breakdown into chlorite and quartz at greenschist facies conditions (≤ 500 °C based on the pseudosection), either during to the cooling stage of the contact metamorphism or more likely during the longer-lived regional metamorphism. Especially, the rounded chlorite poikiloblasts with abundant quartz inclusions are compatible with this interpretation (Fig. 9B). Similar to chlorite, titanite formed after the peak metamorphism at ≤450 °C (Fig. 9A), likely due to reaction between rutile and possibly plagioclase, which could supply the required Ca for the reaction (Fig. 9C). The presence of chlorite and titanite together with the absence of cordierite and muscovite is a strong indication that the Matarakoski black schist around Kevitsa intrusion was subjected to greenschist facies (≤ 500 °C) rather than lower amphibolite facies regional metamorphism, and is also compatible with the previously interpreted border between the two metamorphic zones (Hölttä et al., 2007). In summary, the mineralogical evidence and temperature estimates strongly indicate that the peak metamorphism observed in our samples was caused by contact metamorphism, and not by regional metamorphism.

4.2. *Magma-sediment interaction and contact metamorphism around the sills*

Drill core KV01 provides an opportunity to characterize the style of magma–sediment interaction and contact metamorphism associated with sill intrusions at Kevitsa. These sill intrusions most likely represent magma injections into the black schist, along the flank of the main intrusion (Fig. 10A–B). Based on its low MgO and high TiO_2, REE, and Zr contents (Fig. 8, Table S9), the magma had fractionated extensively within the main intrusion before it intruded the black schist as a sill. We suggest that the sill represents residual melt expelled from the Kevitsa intrusion after the formation of the gabbroic cumulates, which contain only small amount of interstitial melt based on the low incompatible trace element (e.g., Zr and REE) contents (Luolavirta et al., 2018a, 2018b). Within the main intrusion, the parental melt is likely to have undergone extensive black schist assimilation during emplacement, as strongly suggested by Sr, Nd, and S isotopic studies (Grinenko et al., 2003; Huhma et al., 2018; Luolavirta et al., 2018a). This explains the

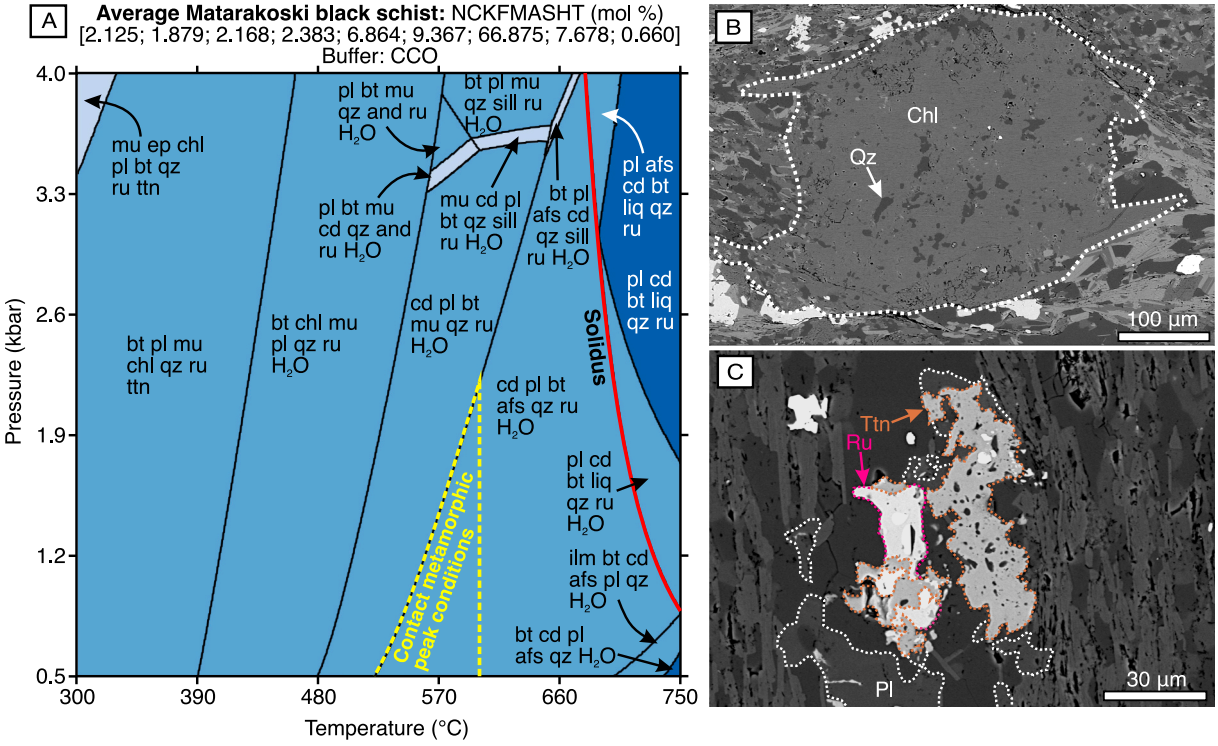

Fig. 9. A) pseudosection calculated in the NCKFMASHT (Na, Ca, K, Fe, Mg, Al, Si, H_2O, Ti) system for the average composition of the Matarakoski black schist using MAGEMin (Riel et al., 2022). The system is buffered to graphite-CO (CCO). The thermodynamic dataset is ds62 (Holland and Powell, 2011) and solution models are from White et al. (2014). For the average black schist calculation, Fe bound to pyrrhotite was removed with the assumption that all sulfur is hosted in $Fe_{0.94}S$, which is close to the observation in the samples. From the average calculation, we omitted sample K09, which has anomalously high CaO (12.2 wt%) and CO_2 (3.74 wt%) contents indicating the presence of carbonates. The colors correspond to the degrees of freedom, which is defined by the number of stable phases within the fields. The peak contact metamorphic conditions have been estimated based on the peak metamorphic temperatures defined using the Raman spectroscopy of carbonaceous materials and based on the absence of muscovite and presence of alkali feldspar in our samples. B) chlorite poikiloblast with quartz inclusions in sample K14. C) Textural association of titanite, rutile, and plagioclase in sample K12. Abbreviations are: afs = alkali feldspar, and = andalusite, bt = biotite, cd = cordierite, chl = chlorite, ep = epidote, ilm = ilmenite, liq = melt, mu = muscovite, pl = plagioclase, qz = quartz, ru = rutile, sill = sillimanite, and ttn = titanite.

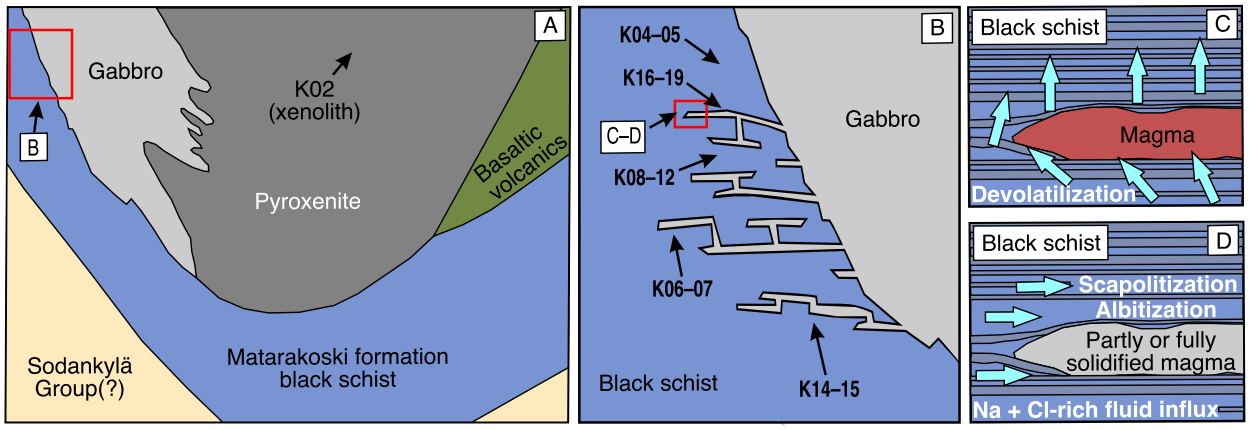

Fig. 10. A) a cross-section of the Kevitsa intrusion and surrounding lithologies modified after Luolavirta et al. (2018c). Note that the presence of the Sodankylä Group has not been verified and that the extent of the Matarakoski formation below the Kevitsa intrusion is uncertain. B) a schematic close-up of the contact zone between the Kevitsa intrusion and the black schist, illustrating a combination of concordant and discordant geometries. The schematic is not to scale, and the exact extent, thickness, and number of sill-like intrusions into the black schist are unknown. Sample locations are approximate and intended to represent relative depth and position below, above, and between the sills. C) a schematic of a sill intruding into the black schist and causing devolatilization of the host rock. D) subsequent influx of Na- and Cl-bearing fluids during either syn- or postmagmatic stage, resulting in scapolitization and albitization of the rocks.

similar primitive mantle normalized REE patterns of the sill and black schist (Fig. 8), although it should be noted that additional assimilation of some deeper country rocks is also possible (Huhma et al., 2018). The sill has higher REE contents than the black schist (Fig. 8), which indicates that extensive fractionation of clinopyroxene, orthopyroxene, and plagioclase occurred within the main intrusion prior to the final emplacement of the sill. Clinopyroxene and orthopyroxene preferentially incorporate HREE over LREE (e.g., Bédard, 2007, 2014), which could explain the slightly more LREE-enriched composition of the sills compared to the black schist.

During the emplacement of the sill, in situ assimilation is markedly more limited and primarily confined to the immediate contact zone (~1 m thick), where the contents of some major elements (SiO_2, TiO_2, $Fe_2O_3^{total}$, and CaO) in the magmatic rocks change towards compositions characteristic of the black schist (Fig. 8). However, interpretations of element fluxes during in situ assimilation remain uncertain due to overprinting albitization in both the gabbroic rocks and the black schist. Only carbon mobilization is clearly observable in the distinct ~8 m-thick, recrystallized, carbon-poor zone above the ~14 m-thick sill. It is likely that most chemical changes within this zone were triggered by devolatilization as the temperatures did not reach the solidus of the black schist based on the pseudosection (Fig. 9A).

The peak temperatures recorded in carbonaceous materials from all sampled black schists are fairly uniform, regardless of the distance from the nearest visible sills (Fig. 5). This suggests that the contact metamorphism of the black schist was primarily driven by the main body of the Kevitsa intrusion. With the exception of the sample K02, which represents a xenolith within the Kevitsa intrusion (Fig. 10A), the highest temperatures are registered in samples K14–15, which come from the deepest sampled parts of the Matarakoski formation (Fig. 3 and 10B), possibly due to the slower cooling of the deeper part of the contact aureole. In conclusion, the extents of assimilation and contact metamorphism around the small and fractionated sills were limited compared to the more pronounced effects within the main Kevitsa intrusion, which supplied significantly more heat. However, we propose that the more extensive devolatilization adjacent to the sills may have generated zones of higher porosity, which channelized the influx of Na- and Cl-rich fluids, resulting in intense biotite-scapolite alteration and albitization (Fig. 10C-D).

4.3. Timing and significance of biotite-scapolite alteration

To estimate the timing of biotite-scapolite alteration in the drill core KV01, we use a Ti-in-biotite thermometer (Henry et al., 2005) to compare the equilibration temperatures of biotite with the peak metamorphic temperatures from the same samples. This Ti-in-biotite thermometer has been calibrated for ilmenite or rutile-bearing graphitic pelites, which experienced regional metamorphism at ~4–6 kbar and 480–800 °C and it has uncertainty of ±25 °C (Henry et al., 2005). The thermometer has been shown to yield reasonable results (within 16 ± 23 °C from other thermometry estimates) for the Ballachulish contact metamorphic aureole with a lower pressure of ~3 kbar (Henry et al., 2005 and references therein). The samples, for which we have measured biotite compositions, have suitable mineral assemblages for the thermometry as they contain carbonaceous materials and minor rutile. Moreover, the measured biotite grains have Mg/(Mg + Fe) and Ti contents (Table S3) in the range of the dataset used for calibrating the thermometer (Henry et al., 2005). The main uncertainty is related to pressure for which we lack any quantitative estimations but it is likely lower than 3 kbar as the Kevitsa intrusion formed during the same late stage of the passive margin basin setting in which the Savukoski Group sediments were originally deposited (see also Fig. 9A). Another Ti-in-biotite thermometer, which was calibrated for similar mineral assemblages and pressure-temperature-composition ranges as the one adopted in this study, indicates that the effect of pressure is linear with the calculated temperature increasing by ~10 °C/kbar (Wu and Chen, 2015). This thermometer was shown to produce within uncertainty same temperatures with the other calibration for all tested mineral assemblages (Wu and Chen, 2015). We consider that our Ti-in-biotite thermometer results may underestimate the temperature at most by 30 °C due to the uncertainty of pressure.

For our four scapolite-bearing black schist samples, the Ti-in-biotite thermometry yields temperatures of 484–563 °C ($n = 2$), 529–598 °C ($n = 6$), 510–567 °C ($n = 3$), and 474–613 °C (n = 6). Most of these temperatures are within uncertainty overlapping with the peak metamorphic temperatures defined for the same samples using the carbonaceous material thermometer (Fig. 11). These results strongly suggest that biotite-scapolite alteration occurred during the peak of contact metamorphism. This interpretation is compatible with our observation that the most pervasive biotite-scapolite alteration is present within a 4-m interval 3–7 m from an intrusive contact, and with the earlier documentation of most intensive scapolitization in the area being spatially associated with the Kevitsa intrusion (Mutanen, 1997). Scapolite in our black schist samples is compositionally close to the Na and Cl-rich endmember marialite, which is typical in the ~50–100 km wide east-west oriented scapolite-alteration district extending from the

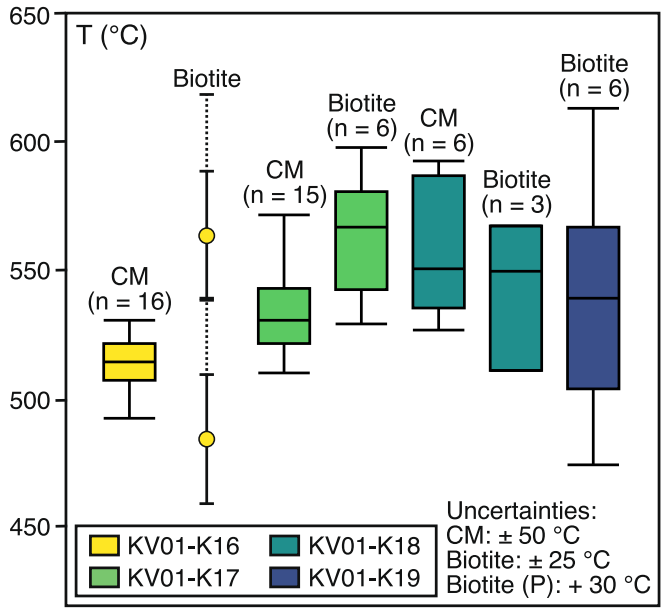

Fig. 11. Comparison with the thermometry results based on the structure of carbonaceous materials (CM) and composition of biotite. No carbonaceous materials were measured from K19 due to too low concentration of carbon. The additional +30 °C uncertainty for the biotite thermometry results is related to the uncertainty in pressure (P) during the contact metamorphism.

eastern border of Finland to the western border of Sweden (Frietsch et al., 1997; Tuisku, 1985). Clearly, the main stage of regional scapolite-alteration must be related to large-scale flow of Cl-rich fluids during orogenic processes rather than localized contact metamorphism. Nevertheless, the presence of scapolite, which formed at the peak contact-metamorphic stage around the Kevitsa intrusion, indicates flow of Cl-rich fluids in the vicinity of the intrusion during the syn- or post-magmatic stage. Flow of Cl-rich fluids within the contact-metamorphosed Matarakoski formation has been previously suggested based on whole-rock Cl-data (Mutanen, 1997). The positive correlation between Cl and K_2O in the contact-metamorphosed Matarakoski formation samples (Mutanen, 1997) is consistent with biotite-scapolite alteration as observed in our study. In previous studies, evaporitic rocks, which are common in the underlying Sodankylä Group, have been suggested as the source of Cl in the fluid (Frietsch et al., 1997; Mutanen, 1997; Tuisku, 1985) but supporting data for the origin of Cl is lacking. A detailed study on Br/Cl in scapolite could reveal the origin of the Cl-rich fluids (see, Qiu et al., 2021; Zeng et al., 2020).

Our findings highlight that Cl-rich fluids were present around the Kevitsa intrusion during the syn- and/or postmagmatic stage. Syn-magmatic mobility of Cl is compatible with the up to wt% level Cl contents in whole-rock samples and the presence of unusually Cl-rich magmatic amphibole, biotite, and apatite in the Kevitsa intrusion (Mutanen, 1997). Scapolite has also been documented from the Kevitsa intrusion (Mutanen, 1997), which indicates that influx of Cl-rich fluids continued in the postmagmatic stage as well. The presence of Cl-rich fluids could be important for the mineralization in Kevitsa as they can mobilize base metals, especially Cu and Co (Liu et al., 2024; Pirajno, 2018). A detailed study on the paragenesis of the Cu and Co-bearing sulfides in the Kevitsa intrusion and their spatial association with the Cl-rich phases could reveal how important the Cl-rich fluids were for the mineralization. Based on the thorough albitization of plagioclase in the black schist and leucogabbro at the contact with biotite-scapolite altered black schist, we speculate that these fluids might have been compositionally similar to those forming the scapolite-albite-associated polymetallic Au—Cu deposits in the northern Fennoscandia (see, Frietsch et al., 1997). A detailed study on the distribution of Cu, Ni, Au, and PGE in the Kevitsa intrusion has shown that Cu and Au have been mobilized in postmagmatic hydrothermal processes (Le Vaillant et al., 2016). We consider it as a possibility that Cl-bearing fluids from the contact-aureole infiltrated the Kevitsa intrusion in both syn- and postmagmatic stages, mobilizing sulfur and metals from the sulfide deposits. However, it should be noted that a later orogeny-related regional scale process cannot be excluded with the existing data.

4.4. *Sulfide genesis in the contact-metamorphosed black schist*

The sulfide-bearing black schist of the Matarakoski formation has been suggested to be the main source of sulfur in the Kevitsa Cu-Ni-PGE sulfide deposits (Grinenko et al., 2003; Luolavirta et al., 2018a; Mutanen, 1997). Sulfur is proposed to be assimilated as the magma partially melted the black schist with graphite in the magmatic rocks representing the solid residue of the digested material (Mutanen, 1997). The possible devolatilization of sulfur from the contact-metamorphosed Matarakoski formation has not been considered in the previous studies. This process was likely important in the formation of the Ni—Cu deposits of Pechenga in Kola Peninsula (Barnes et al., 2001), and the Cu-Ni(-PGE) deposits of the Duluth Complex in Minnesota (Ripley, 1981; Virtanen et al., 2021). The following discussion focuses on the genesis of sulfides in the contact-metamorphosed black schist, with particular emphasis on the role of hydrothermal processes.

Matarakoski black schist occurrences with pyrite concretions and regularly spaced macroscopic pyrite bands of a suggested sedimentary origin have been described between the town of Sodankylä and the Kevitsa intrusion (Hackman, 1927; Mikkola, 1941). Accordingly, we suggest that the pyrrhotite-bearing black schist around the Kevitsa intrusion was likely pyrite-bearing during the onset of the magmatism. This interpretation is compatible with the fact that pyrite commonly forms in black shales during the diagenetic and early metamorphic stages, whereas pyrrhotite is rarely present in these conditions (e.g., Rickard and Morse, 2005; Schoonen, 2004). Pyrrhotite in black schists typically forms in early metamorphic devolatilization stage when pyrite reacts with methane released from the carbonaceous materials (2 pyrite + CH_4 = 2 pyrrhotite +2 H_2S + carbonaceous material). Under water-undersaturated conditions, the decomposition of pyrite is progressive initiating when the metamorphic temperature reaches ~350–400 °C and continuing until ~500–650 °C (Chen et al., 2000; Ma et al., 2016). The regional metamorphism in the Sodankylä area reached ~350–400 °C (Hölttä et al., 2007, Hölttä and Heilimo, 2017), which is compatible with the preservation of the original sedimentary pyrite as observed in the regionally metamorphosed black schists (Hackman, 1927; Mikkola, 1941). Our thermometry results indicate that the pyrrhotite-bearing black schist at the vicinity of the Kevitsa intrusion reached peak contact-metamorphic temperatures of 500–600 ± 50 °C, which would have caused complete pyrite decomposition.

Ubiquitous Ni-bearing pyrrhotite, which is often intergrown with the silicate phases in our black schist samples (Fig. 7B and D) is consistent with the interpretation of it representing residual sulfide after pyrite decomposition. Black shale heating experiments have shown that decomposition of Ni-free pyrite can lead to formation of Ni-bearing pyrrhotite as Ni becomes available from breakdown of chlorite or other phases in the sedimentary rock (Virtanen et al., 2021). Pyrite decomposition mobilizes roughly 50 wt% of sulfur in a fluid phase, which may either re-precipitate in situ within the black schist or propagate via suitable structures to the surroundings such as the adjacent metavolcanic rocks of the Savukoski Group or to the Kevitsa or Satovaara intrusions. Sulfur isotopic composition of sulfides remain largely unchanged during the process (Seal II, 2006). Considering that the maximum apparent distance (observed distance in drill core) of our samples from the intrusive contact is 165 m, the quantity of sulfur that could have been mobilized is large and this could have contributed to the sulfur budget of the Kevitsa deposits. Estimating whether sulfur was gained or lost in the contact metamorphosed black schist is, however,

currently not possible due to the lack of sufficient amount of data to constrain the variability of sulfur content in the regional black schist. Importantly, it is not clear if the sulfide-rich character of the upper portion of the Matarakoski formation black schist, which hosts the Kevitsa intrusion, is a primary sedimentary feature or if it is related to sulfur redistribution within the black schist during contact metamorphism. It is important to emphasize that sulfur assimilation via fluid transport and partial melting are not mutually exclusive processes and both could have contributed to the genesis of the Kevitsa deposits (Mutanen, 1997).

In our black schist samples, chalcopyrite and Co-bearing pyrite are present as inclusions and over- or intergrowths in pyrrhotite (Fig. 7 B and D), which suggests that they are not of primary sedimentary origin, especially as any original pyrite would have decomposed during the contact metamorphism. Based on a compilation of pyrite data from submarine exhalative (SEDEX) and VMS deposits, as well as various sedimentary, magmatic, and skarn rocks, it has been suggested that Co/Ni can be used as a genetic indicator for pyrite (Bajwah et al., 1987). In sedimentary and magmatic rocks, pyrite has generally Co/Ni < 1 with the absolute contents of these metals being higher in pyrite with magmatic origin (Bajwah et al., 1987). Skarns contain pyrite with Co/Ni of 1–10 and highest Co/Ni of 10–50 is found in SEDEX and VMS deposits (Bajwah et al., 1987). In our pyrite, Ni content is below the detection limit of 0.04 wt% and Co content is 0.59–1.57 wt% meaning that minimum Co/Ni is around 15–40, which is similar with pyrite from SEDEX and VMS deposits. In these types of deposits, pyrite precipitates from generally S- and Cl-rich fluids (e.g., Large, 1992), which is consistent with the presence of scapolite in our samples as it indicates presence of Cl-bearing fluids during contact metamorphism. In addition, the relatively Co-poor pyrrhotite also points to hydrothermal origin of Co, which otherwise should have become enriched in pyrrhotite during pyrite decomposition (Finch and Tomkins, 2017).

In addition to Co-pyrite and chalcopyrite, we have identified arsenopyrite, sphalerite and galena in our samples and these minerals are commonly associated with SEDEX and VMS deposits (Large, 1992). Arsenopyrite in our samples has highly variable Co/Ni from 3.2 to 70.0 (average 26.2, $n = 14$). We are not aware of Co-rich arsenopyrite as a primary sedimentary sulfide but it is for example associated with chert and carbonate-hosted hydrothermal Co mineralization in the Eastern Kunlun metallogenic belt in China (Liu et al., 2024). Generally, the observed sulfides (with the exception of pyrrhotite) precipitate at <400 °C, when the metal solubility of the fluid is sufficiently low (Large, 1992), which is much lower compared to the peak metamorphic temperature in our samples. Accordingly, we suggest that chalcopyrite, Co-bearing pyrite, and arsenopyrite precipitated simultaneously with scapolite from a fluid phase during the retrograde stage of contact metamorphism. These observations provide additional evidence for our speculation of Cu and Co mobility in the Cl-bearing fluids during contact-metamorphic fluid circulation in the black schist. As the source of the fluid is unknown, the effect on sulfur isotopic composition of the black schist cannot be evaluated. However, since chalcopyrite, pyrite, and arsenopyrite occur only in minor quantities, the existing whole-rock sulfur isotopic data likely reflects the original sedimentary sulfide signature and can therefore be used reliably to trace the source of sulfur. To summarize, the contact metamorphism of the Matarakoski black schist facilitated sulfur release through large-scale pyrite decomposition to pyrrhotite followed by subsequent flux of Cl-rich fluids, which mobilized Cu and Co in the black schist and potentially in the Kevitsa intrusion.

5. Conclusions

This study provides new constraints on the contact metamorphism of the Matarakoski formation black schist surrounding the Kevitsa and Satovaara intrusions. Peak temperatures reached 500–600 $\pm$ 50 °C in the contact aureole and $\geq$ 650 °C in xenoliths, as determined by Raman spectroscopy of carbonaceous materials. Even adjacent to the sills within the black schist, the peak temperatures seem to be controlled by the main intrusive bodies. Biotite-scapolite alteration of the black schist occurred during the peak contact metamorphic stage, based on Ti-in-biotite thermometry, which indicates influx of Cl-rich fluids within the contact aureole during the syn- or postmagmatic stages. A future study could reveal if these fluids originated from the evaporitic rocks of the area. Albitization adjacent to the biotite-scapolite zones likely occurred during this stage, suggesting a similar fluid composition as for scapolite-albite-associated polymetallic Au deposits in northern Fennoscandia. These fluids were likely channeled through porous zones near sills and contributed to the mobilization of Cu and Co within the black schist and potentially into the Kevitsa intrusion. Such fluid-influx may have played a role in redistributing metals in the Kevitsa Cu-Ni-PGE deposit as well.

Pyrite decomposition to pyrrhotite during contact metamorphism of the black schist led to widespread mobilization of sulfur, which may have contributed to the formation of the Kevitsa Cu-Ni-PGE deposit. The presence of Co-rich pyrite, chalcopyrite, and arsenopyrite in the black schist, suggest that metal redistribution occurred during retrograde metamorphism, probably due to prolonged circulation of the Cl-rich fluids. Overall, our findings support a multi-stage model for the genesis of the Kevitsa Cu-Ni-PGE deposit, involving partial melting, devolatilization, and hydrothermal fluid transport. Further constraints on the extent and style of black schist assimilation by the magma, the sources of Cl-rich fluids, and the sulfur mass balance between regionally and contact-metamorphosed black schist could help refine the role of these processes in ore formation. Our study emphasizes the importance of contact aureole processes in contributing sulfur and mobilizing metals in magmatic sulfide deposits hosted by mafic-ultramafic intrusions.

CRediT authorship contribution statement

V.J. Virtanen: Writing – original draft, Visualization, Validation, Supervision, Methodology, Investigation, Formal analysis, Conceptualization. **H.R. Campos Rodríguez:** Conceptualization, Methodology, Investigation, Writing – review & editing. **S. Yang:** Writing – review & editing, Project administration, Investigation, Funding acquisition. **G. Iacono-Marziano:** Writing – review & editing, Supervision, Methodology, Investigation, Conceptualization. **T. Voipio:** Writing – review & editing, Resources, Investigation. **A. Canizarès:** Writing – review & editing, Supervision, Methodology, Investigation. **Y. Gourseaud:** Writing – review & editing, Methodology, Investigation. **M. Versavel:** Writing – review & editing, Methodology, Investigation. **T. Törmälehto:** Writing – review & editing, Resources.

Declaration of competing interest

During the research conducted for this paper, authors T.V. and T.T. were employed by Boliden Kevitsa, the owner of the Kevitsa Cu-Ni-PGE mine. The other authors declare no financial or non-financial interests.

Acknowledgements

The collaboration of Boliden Kevitsa personnel, especially with Tobias Hermansson, was invaluable to this research. We thank Mikko Savolainen for providing the samples from the GTK repository, Sylvain Janiec for preparing the thin sections, Ida Di Carlo, Saskia Erdmann, and Patricia Benoist for helping with the mineral chemical analyses, and Yiyi Chen for assisting with Raman spectroscopy. This study is supported by the SEMACRET project (101057741) co-funded by Horizon Europe program and UK Research Innovation. We thank Nadia Malaspina for editorial handling, and Dave Good and an anonymous reviewer for their constructive comments.

Appendix A. Supplementary data

Supplementary data to this article can be found online at https://doi.org/10.1016/j.lithos.2026.108511.

References

Aoya, M., Kouketsu, Y., Endo, S., Shimizu, H., Mizukami, T., Nakamura, D., Wallis, S., 2010. Extending the applicability of the Raman carbonaceous-material geothermometer using data from contact metamorphic rocks. J. Metamorph. Geol. 28, 895–914. https://doi.org/10.1111/j.1525-1314.2010.00896.x.

Bajwah, Z.U., Seccombe, P.K., Offer, R., 1987. Trace element distribution, Co: Ni ratios and genesis of the Big Cadia iron-copper deposit, New South Wales, Australia. Mineral. Deposita 300, 292–300.

Barnes, S.J., Melezhik, V.A., Sokolov, S.V., 2001. The composition and mode of formation of the pechenga nickel deposits, Kola Peninsula, Northwestern Russia. Can. Mineral. 39, 447–471. https://doi.org/10.2113/gscanmin.39.2.447.

Bédard, J.H., 2007. Trace element partition coefficients between silicate melts and orthopyroxene: Parameterizations of D variations. Chem. Geol. 244, 263–303. https://doi.org/10.1016/j.chemgeo.2007.06.019.

Bédard, J.H., 2014. Parameterizations of calcic clinopyroxene—Melt trace element partition coefficients. Geochem. Geophys. Geosyst. 15, 303–336 doi:10.1002%2F2013GC005112.

Beyssac, O., Lazzeri, M., 2012. Application of Raman Spectroscopy to the Study of Graphitic Carbons in the Earth Sciences, 12. European Mineralogical Union and the Mineralogical Society of Great Britain & Ireland, pp. 415–454. https://doi.org/10.1180/EMU-notes.12.12.

Beyssac, O., Goffé, B., Chopin, C., Rouzaud, J.N., 2002. Raman spectra of carbonaceous material in metasediments: a new geothermometer. J. Metamorph. Geol. 20, 859–871.

Boliden, 2024. Annual & Sustainability Report 2024. https://investors.boliden.com/sites/boliden-ir/files/pr/202503192744-1.pdf.

Chen, H., Li, B., Zhang, B., 2000. Decomposition of pyrite and the interaction of pyrite with coal organic matrix in pyrolysis and hydropyrolysis. Fuel 79, 1627–1631. https://doi.org/10.1016/S0016-2361(00)00015-6.

Daly, J.S., Balagansky, V.V., Timmerman, M.J., Whitehouse, M.J., 2006. The Lapland-Kola orogen: Palaeoproterozoic collision and accretion of the northern Fennoscandian lithosphere. Geol. Soc. Lond. Mem. 32, 579–598. https://doi.org/10.1144/GSL.MEM.2006.032.01.35.

Eilu, P., 2015. Overview of gold deposits in Finland. In: Maier, W.D., Lahtinen, R., O'Brien, H. (Eds.), Mineral Deposits of Finland. Elsevier, pp. 377–410.

Finch, E.G., Tomkins, A.G., 2017. Pyrite-pyrrhotite stability in a metamorphic aureole: Implications for orogenic gold genesis. Econ. Geol. 112, 661–674. https://doi.org/10.2113/econgeo.112.3.661.

Frietsch, R., Tuisku, P., Martinsson, O., Perdahl, J.A., 1997. Early Proterozoic Cu-(au) and Fe ore deposits associated with regional Na-Cl metasomatism in northern Fennoscandia. Ore Geol. Rev. 12, 1–34. https://doi.org/10.1016/S0169-1368(96)00013-3.

Grinenko, L.N., Hanski, E., Grinenko, V.A., 2003. Formation conditions of the Keivitsa Cu-Ni deposit, northern Finland: evidence from S and C isotopes. Geochem. Int. 40, 154–167.

Hackman, V., 1927. Studien Über Den Gesteinsaufbau Der Kittilä-Lappmark. Bull. de la Commission Geol. de Finlande 79, 1–105.

Hanski, E., Kamenetsky, V.S., 2013. Chrome spinel-hosted melt inclusions in Paleoproterozoic primitive volcanic rocks, northern Finland: evidence for coexistence and mixing of komatiitic and picritic magmas. Chem. Geol. 343, 25–37. https://doi.org/10.1016/j.chemgeo.2013.02.009.

Hanski, E.J., Luo, Z.-Y., Oduro, H., Walker, R.J., 2011. The Pechenga Ni-Cu Sulfide Deposits, Northwestern Russia: a Review with New Constraints from the Feeder Dikes. Rev. Econ. Geol. 17, 145–162.

Haverinen, J., 2020. Evaporites in the Central Lapland Greenstone Belt. Master's thesis. University of Helsinki, p. 73.

Henry, D.J., Guidotti, C.V., Thomson, J.A., 2005. The Ti-saturation surface for low-to-medium pressure metapelitic biotites: implications for geothermometry and Ti-substitution mechanisms. Am. Mineral. 90, 316–328. https://doi.org/10.2138/am.2005.1498.

Holland, T.J.B., Powell, R., 2011. An improved and extended internally consistent thermodynamic dataset for phases of petrological interest, involving a new equation of state for solids. J. Metamorph. Geol. 29, 333–383. https://doi.org/10.1111/j.1525-1314.2010.00923.x.

Hölttä, P., Heilimo, E., 2017. Metamorphic map of Finland. In: Nironen, M. (Ed.), Bedrock of Finland at the Scale 1:1 000 000 - Major Stratigraphic Units, Metamorphism and Tectonic Evolution, 60. Geological Survey of Finland, Special Paper, pp. 77–128.

Hölttä, P., Väisänen, M., Väänänen, J., Manninen, T., 2007. Paleoproterozoic metamorphism and deformation in Central Lapland, Finland. In: Ojala, V.J. (Ed.), Gold in the Central Lapland Greenstone Belt. Geological Survey of Finland, Special Paper 44, pp. 7–57.

Huhma, H., Hanski, E., Kontinen, A., Vuollo, J., Lahaye, Y., 2018. Sm-Nd and U-Pb isotope geochemistry of the Palaeoproterozoic mafic magmatism in eastern and northern Finland. Bull. Geol. Surv. Finland 405, 150–p.

Huyck, H.L.O., 1991. When is a Metalliferous Black Shale Not a Black Shale. In: Grauch, R.I., Huyck, H.L.O. (Eds.), Metalliferous Black Shales and Related Ore Deposits– Proceedings, 1989 United States Working Group Meeting, International Geological Correlation Program Project 254. U.S. Geological Survey Circular 1058, pp. 42–56.

Korkalo, T., 2006. Gold and Copper Deposits in Central Lapland, Northern Finland, with Special Reference to their Exploration and Exploitation. Doctoral dissertation. University of Oulu, p. 122.

Köykkä, J., Lahtinen, R., Huhma, H., 2019. Provenance evolution of the Paleoproterozoic metasedimentary cover sequences in northern Fennoscandia: age distribution, geochemistry, and zircon morphology. Precambrian Res. 331, 105364. https://doi.org/10.1016/j.precamres.2019.105364.

Lahfid, A., Beyssac, O., Deville, E., Negro, F., Chopin, C., Goffé, B., 2010. Evolution of the Raman spectrum of carbonaceous material in low-grade metasediments of the Glarus Alps (Switzerland). Terra Nova 22, 354–360. https://doi.org/10.1111/j.1365-3121.2010.00956.x.

Lahtinen, R., Korja, A., Nironen, M., 2005. Palaeoproterozoic tectonic evolution of the Fennoscandian Shield. In: Lehtinen, M., Nurmi, P.A., Rämo, O.T. (Eds.), Precambrian Geology of Finland – Key to the Evolution of the Fennoscandian Shield. Elsevier B.V, Amsterdam, pp. 481–532.

Large, R., 1992. Australian Volcanic-Hosted massive Sulfide deposits: features, styles, and genetic models. Econ. Geol. 87, 471–510.

Le Vaillant, M., Barnes, S.J., Fiorentini, M.L., Santaguida, F., Törmänen, T., 2016. Effects of hydrous alteration on the distribution of base metals and platinum group elements within the Kevitsa magmatic nickel sulphide deposit. Ore Geol. Rev. 72, 128–148. https://doi.org/10.1016/j.oregeorev.2015.06.002.

Lehtonen, M., Airo, M., Eilu, P., Hanski, E., Kortelainen, V., Lanne, E., Manninen, T., Rastas, P., Räsänen, J., Virransalo, P., 1998. Kittikän vihreäkivialueen geologia, 140. Geological Survey of Finland Report of Investigation, p. 144.

Liu, T., Jiang, S.Y., Cao, S., Wang, W., Su, H.M., Yang, D., Li, H., He, S., 2024. Cobalt enrichment and metallogenic mechanism of the Galinge skarn iron deposit in the Eastern Kunlun metallogenic belt, western China. Ore Geol. Rev. 170, 106147. https://doi.org/10.1016/j.oregeorev.2024.106147.

Lünsdorf, N.K., Dunkl, I., Schmidt, B.C., Rantitsch, G., von Eynatten, H., 2014. Towards a higher Comparability of Geothermometric Data obtained by Raman Spectroscopy of Carbonaceous Material. Part I: Evaluation of Biasing Factors. Geostand. Geoanal. Res. 38, 73–94. https://doi.org/10.1111/j.1751-908X.2013.12011.x.

Luolavirta, K., Hanski, E., Maier, W., Lahaye, Y., O'Brien, H., Santaguida, F., 2018a. In situ strontium and sulfur isotope investigation of the Ni-Cu-(PGE) sulfide ore-bearing Kevitsa intrusion, northern Finland. Mineral. Deposita 53, 1019–1038. https://doi.org/10.1007/s00126-018-0792-6.

Luolavirta, K., Hanski, E., Maier, W., Santaguida, F., 2018b. Whole-rock and mineral compositional constraints on the magmatic evolution of the Ni-Cu-(PGE) sulfide ore-bearing Kevitsa intrusion, northern Finland. Lithos 296–299, 37–53. https://doi.org/10.1016/j.lithos.2017.10.015.

Luolavirta, K., Hanski, E., Maier, W., Santaguida, F., 2018c. Characterization and origin of dunitic rocks in the Ni-Cu-(PGE) sulfide ore-bearing Kevitsa intrusion, northern Finland: Whole-rock and mineral chemical constraints. Bull. Geol. Soc. Finl. 90, 5–32. https://doi.org/10.17741/bgsf/90.1.001.

Ma, X., Zheng, J., Zheng, G., Xu, W., Qian, Y., Xia, Y., Wang, Z., Wang, X., Ye, X., 2016. Influence of pyrite on hydrocarbon generation during pyrolysis of type-III kerogen. Fuel 167, 329–336. https://doi.org/10.1016/j.fuel.2015.11.069.

Maier, W.D., Barnes, S.J., 2010. The Kabanga Ni sulfide deposits, Tanzania: II. Chalcophile and siderophile element geochemistry. Mineral. Deposita 45, 443–460. https://doi.org/10.1007/s00126-010-0283-x.

Mikkola, E., 1941. Muonio-Sodankylä-Tuntsajoki Explanation to the Map of Rocks. In: The General Geological Map of Finland. Suomen Geologinen Toimikunta, Helsinki, p. 286.

Mutanen, T., 1997. Geology and ore petrology of the Akanvaara and Koitelainen mafic layered intrusions and the Keivitsa-Satovaara layered complex, northern Finland. Bull. Geol. Soc. Finl. 395, 233.

Palme, H., O'Neill, H., 2013. Cosmochemical estimates of Mantle Composition. In: Treatise on Geochemistry: Second Edition. Elsevier Ltd, pp. 1–39. https://doi.org/10.1016/B978-0-08-095975-7.00201-1.

Pirajno, F., 2018. Halogens in Hydrothermal Fluids and their Role in the Formation and Evolution of Hydrothermal Mineral Systems. In: Harlov, D., Aranovich, L. (Eds.), The Role of Halogens in Terrestrial and Extraterrestrial Geochemical Processes. Springer, pp. 759–804. https://doi.org/10.1007/978-3-319-61667-4_12. Springer Geochemistry.

Qiu, Z., Fan, H.R., Tomkins, A.G., Brugger, J., Etschmann, B., Liu, X., Xing, Y., Hu, Y., 2021. Insights into salty metamorphic fluid evolution from scapolite in the Trans-North China Orogen: implication for ore genesis. Geochim. Cosmochim. Acta 293, 256–276. https://doi.org/10.1016/j.gca.2020.10.030.

Queffurus, M., Barnes, S.J., 2014. Selenium and sulfur concentrations in country rocks from the Duluth complex, Minnesota, USA: implications for formation of the Cu-Ni-PGE sulfides. Econ. Geol. 109, 785–794. https://doi.org/10.2113/econgeo.109.3.785.

Räsänen, J., Huhma, H., 2001. U-Pb datings in the sodankylä schist area, central finnish lapland. Geol. Surv. Finland, Spec. Paper 33, 153–189.

Rickard, D., Morse, J.W., 2005. Acid volatile sulfide (AVS). Mar. Chem. 97, 141–197. https://doi.org/10.1016/j.marchem.2005.08.004.

Riel, N., Kaus, B.J.P., Green, E.C.R., Berlie, N., 2022. MAGEMin, an efficient Gibbs energy minimizer: application to igneous systems. Geochem. Geophys. Geosyst. 23, 1–27. https://doi.org/10.1029/2022GC010427.

Ripley, E.M., 1981. Sulfur Isotopic Studies of the Dunka Road Cu-Ni Deposit, Duluth complex, Minnesota. Econ. Geol. 76, 610–620.

Sayab, M., Lahtinen, R., Köykkä, J., Hölttä, P., Karinen, T., Niiranen, T., Leväniemi, H., 2021. Improved resolution of paleoproterozoic orogenesis: Multi-directional

collision tectonics in the sodankylä belt of northern Finland. Precamb. Res 359, 106193. https://doi.org/10.1016/j.precamres.2021.106193.
Schoneveld, L., Barnes, S.J., Luolavirta, K., Hu, S., Verrall, M., Le Vaillant, M., 2025. Extent and survival of zoned pyroxene within intrusions hosting magmatic sulfides: implications for zoned pyroxene as a prospectivity indicator. Mineral. Deposita 60, 533–549. https://doi.org/10.1007/s00126-024-01292-1.
Schoonen, M.A.A., 2004. Mechanisms of sedimentary pyrite formation. Geol. Soc. Am. Spec. Pap. 379, 117–134. https://doi.org/10.1130/0-8137-2379-5.117.
Seal II, R.R., 2006. Sulfur isotope geochemistry of sulfide minerals. Rev. Mineral. Geochem. 61, 633–677. https://doi.org/10.2138/rmg.2006.61.12.
Tuisku, P., 1985. The origin of scapolite in the Central Lapland schist area, northern Finland; preliminary results. Bull. Geol. Soc. Finl. 331, 159–173.
Virtanen, V.J., Heinonen, J.S., Molnár, F., Schmidt, M.W., Marxer, F., Skyttä, P., Kueter, N., Moslova, K., 2021. Fluids as primary carriers of sulphur and copper in magmatic assimilation. Nat. Commun. 12, 6609. https://doi.org/10.1038/s41467-021-26969-3.
Tyrväinen, A., 1983. Sodankylän Ja Sattasen Kartta-Alueiden kallioperä. Summary: Pre-Quaternary Rocks of the Map Sheet Areas of Sodankylä and Sattanen. Geological Map of Finland 1: 100 000. Geological Survey of Finland, Espoo, p. 59.
Virtanen, V.J., Heinonen, J.S., Märki, L., Galvez, M.E., Molnár, F., 2024. Sedimentary and metamorphic processes priming black shale for magmatic assimilation of sulfur: an example from the Virginia Formation, Minnesota, United States. Mineral. Deposita 60, 303–319. https://doi.org/10.1007/s00126-024-01268-1.
White, R.W., Powell, R., Holland, T.J.B., Johnson, T.E., Green, E.C.R., 2014. New mineral activity-composition relations for thermodynamic calculations in metapelitic systems. J. Metamorph. Geol. 32, 261–286. https://doi.org/10.1111/jmg.12071.
Wu, C.-M., Chen, H.-X., 2015. Revised Ti-in-biotite geothermometer for ilmenite- or rutile-bearing crustal metapelites. Sci. Bull. 60, 116–121. https://doi.org/10.1007/s11434-014-0674-y.
Zeng, L.P., Zhao, X.F., Hammerli, J., Fan, T.W.T., Spandler, C., 2020. Tracking fluid sources for skarn formation using scapolite geochemistry: an example from the Jinshandian iron skarn deposit, Eastern China. Mineral. Deposita 55, 1029–1046. https://doi.org/10.1007/s00126-019-00914-3.